Perturbation dynamics of a planktonic ecosystem

by

Katherine Margaret Healey

BSc, University of Victoria, 2005

A Thesis Submitted in Partial Fulfillment of the
Requirements for the Degree of

Master of Science

in the School of Earth and Ocean Sciences

Perturbation dynamics of a planktonic ecosystem

by

Katherine Margaret Healey

BSc, University of Victoria, 2005

Supervisory Committee

Dr. Adam H. Monahan, Supervisor (School of Earth and Ocean Sciences)

Dr. Debby Ianson, Co-Supervisor (School of Earth and Ocean Sciences)

Dr Kenneth L. Denman, Departmental Member (School of Earth and Ocean Sciences)

Supervisory Committee

Dr. Adam H. Monahan, Supervisor (School of Earth and Ocean Sciences)

Dr. Debby Ianson, Co-Supervisor (School of Earth and Ocean Sciences)

Dr Kenneth L. Denman, Departmental Member (School of Earth and Ocean Sciences)

Abstract

Planktonic ecosystems provide a key mechanism for the transfer of CO_2 from the atmosphere to the deep ocean via the so-called "biological pump". Mathematical models of these ecosystems have been used to predict CO_2 uptake in surface waters, and more recently have been embedded in global climate models. While the equilibrium properties of these models are well studied, less attention has been paid to their response to external perturbations, despite the fact that as a result of the variability of environmental forcing such ecosystems are rarely, if ever, in equilibrium. Human induced perturbations to these ecosystems, namely the addition of limiting nutrients (e.g. iron) to areas where nitrate is plentiful to accelerate the biological pump, have been proposed as a solution to reduce atmospheric CO_2. Linear theory is used to determine the structure of "unit-norm" perturbations (size in $mmolNm^{-3}$) to state variables of an ecosystem model in steady state, describing Ocean Station P (50°N

145°W) in summer, that optimize either instantaneous export flux of organic matter at fixed times or integrated export as the ecosystem relaxes towards equilibrium. For all perturbations, the flux to higher trophic levels is the primary contributor to export flux, the contribution of aggregation is negligible, and (sinking) detritus increases significantly in the transient dynamics. Two perturbations considered optimize instantaneous export flux; both perturbations synchronize P_1 and Z_1 relative to their predator prey cycle, resulting in a maximum instantaneous export flux of $4.4 mmol N m^{-2} d^{-1}$, and also increased integrated export above that at steady state ($6 g C m^{-2}$ over 150 days). An increase in larger phytoplankton (P_2), representing diatoms, results in the highest integrated export ($7 g C m^{-2}$). The perturbations in which P_2 persist the longest give the highest integrated export, and these perturbations are primarily increases in P_2. The additional integrated export in response to a proportional increase to steady state concentrations of both large and small phytoplankton is positive, but much lower than the optimal perturbations. However, the additional integrated export in response to an increase in only P_1 is negligible. The linear and nonlinear ecosystem and export responses to two perturbations are compared; for perturbations of magnitude $0.5 mmol N m^{-3}$, the linearization of the ecosystem dynamics, rather than of the export flux, is the primary cause for differences between the fully linear and fully nonlinear cases.

Table of Contents

List of Tables

List of Figures

Acknowledgements

I thank my advisors Dr. Adam Monahan and Dr. Debby Ianson for their continued support, encouragement, patience, and guidance. Adam's enthusiasm for science is contagious, and Debby was always available with thoughtful comments and answers to my questions. I would also like to thank Dr. Ken Denman, Dr. Andrew Edwards, Julie Alexander, the School of Earth and Ocean Sciences staff, and the UVic biogeochemical discussion group for their feedback and support. I am grateful to my course instructors for their feedback and assistance while I developed my academic writing skill. A special thanks goes to my family, particularly Margaret and David Healey, and Robin Bowerman, for their support and patience.

Chapter 1

Introduction

1 Background

Atmospheric CO_2 dissolves in the surface waters of the oceans, and phytoplankton fix some of this CO_2 through photosynthesis, transforming it into particulate organic carbon (POC). A portion of this POC, denoted exported carbon, descends below the mixed layer in the form of dead cells and fecal pellets of zooplankton, and eventually reaches the deep ocean, where it remains essentially out of contact with the atmosphere on climate time scales (i.e. 1000 years). This process is known as the "biological pump", and enhances the ocean's ability to store carbon (Sarmiento and Gruber, 2006, Volk and Hoffert, 1985). Although phytoplankton growth is often limited by light or nutrients, it is not, in general, limited by carbon, and an increase in atmospheric CO_2 will not directly accelerate the biological pump.

There are large areas of the ocean where major nutrients that are often considered limiting to photosynthesis (e.g. N) are available, but there is little phytoplankton biomass. These are called high nutrient low chlorophyll (HNLC) regions, and include

the subarctic North Pacific and Southern Ocean (de Baar et al., 2005). Martin et al. (1989, 1991) hypothesized that phytoplankton growth in HNLC regions is limited by the micronutrient iron, and it has been suggested that atmospheric CO_2 may be reduced by fertilizing HNLC areas with iron to enhance the biological pump. An increase in phytoplankton biomass has been observed following both natural (e.g. Jo et al., 2007) and synthetic (e.g. Saito et al., 2006) iron fertilization events, however exported carbon in response to these events may only be measured indirectly (e.g. Wong et al., 2006). In general, these blooms are not occupied long enough to observe responses in export; thus the effect of iron fertilization on export dynamics remains uncertain.

Because of the importance of export dynamics and possible changes to these dynamics under climate change, it is necessary to develop mechanistic and predictive models of planktonic ecosystem dynamics. Such models typically consist of a system of differential equations describing the temporal evolution of ecosystem variables (e.g. nutrients, phytoplankton, zooplankton (Fasham, 1993)). Real planktonic systems involve a large number of species displaying a bewildering complexity of physiological states, nutrient requirements, and trophic interactions. In contrast, in planktonic ecosystem models, each species of plankton is not modeled individually: rather, phytoplankton and zooplankton are divided into what are termed 'functional groups', defined by common ecosystem-scale characteristics.

Many formulations for modeling ecosystem dynamics have been proposed, and ecosystem models varying in complexity from 3 state variables (nutrient, phytoplankton (P), zooplankon (Z)) in a homogenous medium (e.g. Steele, 1974) to 3-

dimensional models containing multiple functional groups of plankton and nutrients (e.g. Moore et al., 2004) have been studied. Although many comprehensive global climate models that are used to study climate change and the carbon cycle have an ocean biology component that includes a simple planktonic ecosystem model (e.g. Schmittner et al., 2005, Zahariev et al., 2008), the dynamics of these ecosystem models are often poorly understood, particularly their response to a variable physical environment. While the nonlinearity of these model equations generally limits the analytical study of model dynamics, useful insight regarding model dynamics can often be obtained through the study of local linearized dynamics around model equilibria (Perko, 2001). Continual physical forcing from the atmosphere and ocean mean that these ecosystems are never in steady state (Monahan and Denman, 2004). If variability is not too large, the state of the ecosystem may be considered as a steady background state that is modified by some perturbation evolving according to locally linear dynamics. Such a linearization allows for a systematic analysis of the model dynamics for a small perturbation from steady state, and may provide qualitative information about the behaviour of perturbations that may not be considered "small". Locally linearized dynamics have been used to study the stability properties of model equilibria (e.g. Edwards and Brindley, 1999), but although phytoplankton populations display rapid transient growth, less attention has been paid to the dynamics of perturbations around steady states (e.g. Pitchford and Brindley, 1999, Truscott and Brindley, 1994). The relationship between the evolution of ecosystems and export flux is complicated, and possibly counter-intuitive. Well established mathematical theory (e.g. Tziperman and Ioannou, 2002) may be used to determine perturbations

to a steady state that lead to responses from the ecosystem that are "optimal" in some specified way, such as maximizing the export flux (rate of POC leaving the model domain). These perturbations represent small changes to an ecosystem state that occur in response to the addition of iron by dust deposition or advection and mixing with an eddy that has a different concentration of state variables.

This study considers the dynamics of a model designed to simulate ecosystem processes at Ocean Station P (50°N 145°W), a HNLC region located in the subarctic northeast Pacific, where spring and summertime photosynthetic growth is thought to be limited by micronutrients such as iron. In this region, small phytoplankton are dominant and tightly coupled with microzooplankton, and diatom blooms are observed only occasionally (Boyd and Harrison, 1999). This region is studied because a wealth of historical data exists, and Station P was the site of the Subarctic Ecosystem Response to Iron Enrichment Study (SERIES), a synthetic iron fertilization experiment (Boyd et al., 2004). Data from Station P suggest that considerable variability exists in these ecosystems (Wong et al., 1999), although total chlorophyll generally remains approximately constant throughout the year. Most of the time, the ecosystem at Station P appears to be near, or fluctuating about, steady state, and thus this setting is ideal for the analysis of small perturbations to equilibrium.

2 Outline of thesis research

The model used in this study is based on Monahan and Denman (2004) (MD04); the model equations, dynamics, and equilibria are discussed in Chapter 2. This model has a single stable steady state for the parameters under consideration, and this is the state to which perturbations are considered. The perturbations to model state

variables that optimize transient export flux and integrated export are determined in Chapter 3, and the ecosystem and export responses to these perturbations, as well as two additional instantaneous blooms in phytoplankton alone that do not optimize export flux, are discussed in Chapter 4. The ecosystem responses to these perturbations are compared and discussed in Chapter 5, and conclusions are presented in Chapter 6.

The structure of perturbations that optimize instantaneous export flux are solved for; these perturbations provide insight into how different components of a planktonic ecosystem model can be synchronized to produce events of high instantaneous export. These perturbations may be restricted to certain state variables, such as the phytoplankton; I investigate if such a restriction has any effect on the maximum attainable export flux, and compare the ecosystem and export responses to these two perturbations. Although these perturbations produce high instantaneous export flux at some time, they do not guarantee high integrated export, that is, the total amount of POC exported as the ecosystem returns to equilibrium. To investigate if producing a period of high instantaneous export flux is the most efficient way to increase total exported POC, I characterize the perturbation that optimizes integrated export. The ecosystem and export responses to these perturbations may highlight ecosystem dynamics that may not immediately be apparent from the equations that define the ecosystem model. Because these perturbations all optimize export in some way, the ecosystem and export responses may all share some common properties. To elucidate these common traits, I compare the responses of the optimal perturbations to responses of two other perturbations: a proportional increase in both phytoplankton

functional groups, and and increase in only small phytoplankton. Because ecosystem and export responses are linearized about a steady state, I analyze the errors introduced by these approximations, and their effects on export calculations.

Chapter 2

Model

1 Model equations

The planktonic ecosystem model used in this study is based on MD04, but set in a 0-dimensional physical framework, i.e., a uniform mixed layer of fixed depth. This type of model is similar to those used in global models of the carbon cycle (e.g. Zahariev et al., 2008). There are 2 functional groups of phytoplankton; small ($\leq 20\mu m$) phytoplankton, including flagellates (P_1), and large ($> 20\mu m$) phytoplankton, mainly diatoms (P_2). The phytoplankton is split into functional groups because small and large phytoplankton are grazed at different trophic levels, and P_2 are thought to be the most important contributor to export flux. Microzooplankton (Z_1) are modeled explicitly, and are tightly coupled with their prey, which are small phytoplankton and dead organic matter, termed detritus (D). Mesozooplankton (Z_2) graze on larger prey items, which in this model are P_2 and Z_1 (Figure 2.1); Z_2 biomass is not thought to be strongly coupled with prey availability, and is specified at the maximum value of the observed annual cycle (Goldblatt et al., 1999) in order to simulate summer

conditions. The only nutrient explicitly modeled, and so the only potentially limiting nutrient in the model, is nitrogen (N). The evolution of these five state variables is given by the following set of differential equations:

$$\frac{dP_1}{dt} = \nu P_1 - \gamma_1 \frac{P_1}{P_1 + p_D D} Z_1 \tag{2.1}$$

$$\frac{dP_2}{dt} = \nu P_2 - \gamma_2 Z_2 \frac{P_2}{P_2 + Z_1} - m_{pd} P_2 - w_A (P_2^2 + \frac{2P_2}{P_2 + D} P_2 D) \tag{2.2}$$

$$\frac{dZ_1}{dt} = g_a \gamma_1 Z_1 - \gamma_2 Z_2 \frac{Z_1}{P_2 + Z_1} - m_{za} Z_1 \tag{2.3}$$

$$\frac{dD}{dt} = m_{pd} P_2 + (1 - g_a)\gamma_1 Z_1 - \gamma_1 \frac{p_D D}{P_1 + p_D D} Z_1 - r_e D - w_D D - w_A (D^2 + \frac{2D}{P_2 + D} P_2 D) \tag{2.4}$$

$$\frac{dN}{dt} = -\nu(P_1 + P_2) + r_e D + m_{za} Z_1 + m_{ca} \gamma_2 Z_2 + \frac{v_{UW}}{d_{ML}} (N_0 - N) \tag{2.5}$$

Table 2.1 contains definitions of symbols that are frequently used in this study, including state variables. Parameter values are given in Table 2.2.

The phytoplankton specific growth rate, ν, is given by Liebig's law of the minimum:

$$\nu = \nu_{max} min(\frac{N}{k_n + N}, L_{fe}) \tag{2.6}$$

where ν_{max} is the maximum growth rate in the absence of nutrient limitation and

k_N is a nitrogen half-saturation constant. When growth is not limited by N, the parameter L_{fe} sets an upper limit on phytoplankton growth that represents limitation of a micronutrient such as iron. Because the model is set in summer conditions, it is assumed that light is not limiting at any time.

The microzooplankton, Z_1, graze on both P_1 and D with grazing rate

$$\gamma_1 = r_m \frac{(P_1 + p_D D)^2}{k_p^2 + (P_1 + p_D D)^2} \tag{2.7}$$

where p_D is the relative grazing preference of Z_1 on D over P_1 and k_p is the "half-saturation constant". Many parameterizations of zooplankton grazing have been considered (e.g. Gentleman et al., 2003); most of these formulations are chosen so that grazing rates decrease when little prey is available, and saturate to a maximum when there is an abundance of prey. The use of quadratic zooplankton grazing formulation, as in Equation 2.7, is common to many ecosystem models (e.g. Steele and Henderson, 1992).

Mesozooplankton biomass is held fixed because Z_2 have relatively long life spans, and biomass is unlikely to change in response to ecosystem changes on the time scales considered. However, the Z_2 grazing rate responds to changes in availability of P_2 and Z_1:

$$\gamma_2 = r_c \frac{(P_2 + Z_1)^2}{k_z^2 + (P_2 + Z_1)^2} \tag{2.8}$$

The mortality rate of P_2 to D, m_{pd}, is linear. Aggregation, i.e. the formation of marine snow (Alldredge and Silver, 1988), is represented by a quadratic term in

both P_2 and D. The assimilation efficiency of Z_1, i.e. the portion of grazed P that is converted to Z biomass, is denoted g_a; unassimilated matter, e.g. biomass lost to sloppy feeding, becomes D. Microzooplankton excrete N with specific rate m_{za}. The particulate nitrogen contained in detritus is converted to dissolved nitrogen at the specific remineralization rate r_e, and D sinks at rate w_D ($7.5md^{-1}$). A portion of the biomass grazed by Z_2 is immediately excreted to N at a rate of m_{ca}

Station P is located in the Alaskan Gyre; this gyre flows "counterclockwise", thus Ekman transport causes water to be pushed away from the gyre center, causing surface divergence that results in weak upwelling (Pond and Pickard, 1983). Nitrogen is injected via upwelling and exchanged by mixing, with water from below the mixed layer that has average nitrogen concentration N_0 at rate v_{UW}. Any dilution of other state variables by physical exchange is included in the linear growth and mortality rates. The physical parameters for the model are set to be broadly consistent with observations made at Station P in the summer, where these observations exist (Table 2.2).

There are 3 pathways for the export of particulate matter from the ecosystem: sinking D (with no aggregation), flux to higher trophic levels as P_2 and Z_1 are grazed upon by Z_2, and aggregation of P_2 and D (Figure 2.1, Equations 2.2, 2.3, and 2.4). The third export pathway simulates the formation of marine snow in which larger phytoplankton and detritus form aggregates, which then sink rapidly (Alldredge and Silver, 1988). Denman et al. (2006) included aggregates composed only of large phytoplankton; the inclusion of aggregated detritus in this model increases the contribution of small phytoplankton to the flux of sinking particles (Richardson and

Jackson, 2007).

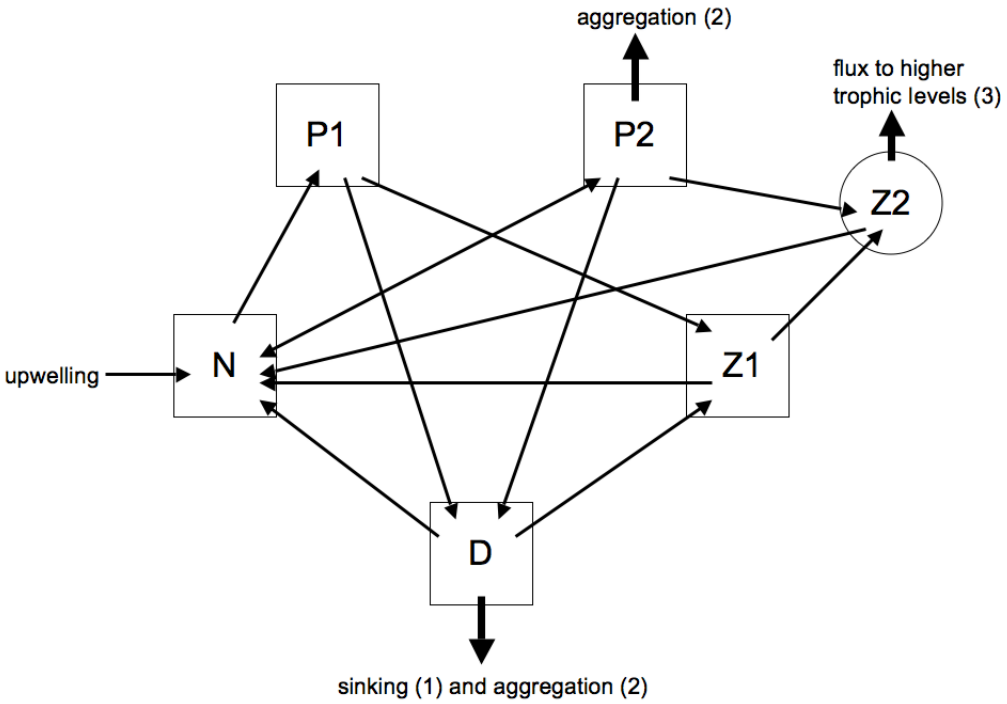

Figure 2.1: Model dynamics. State variables include nitrogen (N), small phytoplankton (P1), large phytoplankton (P2), small zooplankton (Z1), large zooplankton (Z2, prescribed state variable), and detritus (D). Bold arrows denote export: detritus sinks (1), detritus and large phytoplankton form aggregates (2), and large phytoplankton and small zooplankton are consumed by large zooplankton (3). In steady state these losses are balanced by the input of N via upwelling.

2 Steady states

Four steady states for this model were found (Table 2.3) using the fsolve routine in MATLAB, which solves for roots of systems of nonlinear equations. The first

t	time
P_1	Small phytoplankton ($\leq 20\mu m$)
P_2	Large phytoplankton ($> 20\mu m$)
Z_1	Microzooplankton
D	Detritus
N	Nitrogen
Z_2	Mesozooplankton
Φ_{FLUX}	Maximizes instantaneous export flux, amplification
Φ_{FLUX-P}	Maximizes instantaneous export flux, amp.; restricted to P_1 and P_2
Φ_{INT}	Maximizes integrated export
Φ_{P_2}	Increase in only P_2
$\Phi_{P_1P_2}$	Proportional increase in P_1 and P_2
Φ_{P_1}	Increase in only P_1

Table 2.1: Definition of frequently used symbols

of these equilibria has zero values of P_1, P_2, Z_1 and D; the only nonzero state variable is N. The second steady state has no P_1 or Z_1, but nonzero P_2 and D. All state variables are nonzero in the third steady state, and in the fourth all but P_2 are nonzero. Of all steady states, only steady state 3 is stable, that is, small perturbations to this equilibrium will result in a return to this state; it also corresponds to a reasonable representation of conditions at Station P. Observations taken in the late summer suggest the phytoplankton community is 80% P_1 and 20% P_2 by mass, and the total phytoplankton biomass is about $0.3 mmol N m^{-3}$ (Boyd and Harrison, 1999). Compared to the few data that exist, the ratio of P_1 to P_2 at steady state agrees with observations, but there is roughly twice as much phytoplankton at steady state than these observations suggest. We do not expect the values (model steady state and observed) to be identical; differences likely occur because the model is an idealized and simplified representation of ecosystem dynamics, and the ecosystem

		Value	Unit	Source
ν_{max}	maximum phyto. growth rate	1.5	d^{-1}	DP02
p_d	grazing preference of Z_1 on D	0.5	-	DP02
Z_2	Z_2 biomass	0.2	$mmolNm^{-3}$	DP02
m_{pd}	P_2 to D mortality	0.1	d^{-1}	MD04
m_{za}	Z_1 to N	0.1	d^{-1}	MD04
r_e	D remineralization rate	0.1	d^{-1}	DP02
m_{ca}	Z_2 grazing to N	0.3	-	DP02
r_m	maximum Z_1 grazing rate	1.0	d^{-1}	DP02
k_p	Z_1 grazing half-saturation const.	0.75	$mmolNm^{-3}$	DP02
r_c	maximum Z_2 grazing rate	6.5	d^{-1}	MD04
k_z	Z_2 grazing half-saturation const.	2	$mmolNm^{-3}$	MD04
N_0	average N below mixed layer	26.8	$mmolNm^{-3}$	P-Hist
k_n	P growth half-saturation const.	0.1	$mmolNm^{-3}$	DP02
L_{fe}	iron limitation coefficient	0.05	-	tuned
d_{ML}	mixed layer depth	20	m	W99
v_{uw}	upwelling velocity	.1	md^{-1}	A93
w_D	D turnover rate due to sinking	0.3750	d^{-1}	MD04
g_a	Z_1 assimilation efficiency	0.7	-	DP02
w_A	aggregation coefficient	0.02	$mmolN^{-1}m^3d^{-1}$	I08

Table 2.2: Model parameter values. Many ecosystem parameters have been tuned to agree with observations and are not well constrained. MD04=Monahan and Denman (2004), DP02=Denman and Pena (2002), W99=Whitney and Freeland (1999), A93= Archer et al. (1993) , I08= Ianson et al. (in prep), P-Hist=Station P historical data, Institute of Ocean Sciences Archive

	steady state values ($mmolNm^{-3}$)			
	1	2	3	4
P_1	0.0000	0.0000	**0.5265**	0.4907
P_2	0.0000	0.4853	**0.1105**	0.0000
Z_1	0.0000	0.0000	**0.4073**	0.4173
D	0.0000	0.1010	**0.0919**	0.0677
N	26.8000	7.7252	**8.3153**	14.1096

Table 2.3: Steady state values found for the ecosystem model. Bold font indicates stable equilibria.

is never in steady state in the ocean, so observations are not taken at equilibrium. The perturbation dynamics around this equilibrium will be the focus of this study. The other steady states are unstable because all have at least one phytoplankton functional group not present, such that even a small increase in either functional group of phytoplankton will result in further growth.

3 Export dynamics

Export from the ecosystem is given by the equation

$$Export = w_D D + \gamma_2 Z_2 + w_A (P_2 + D)^2 \tag{2.9}$$

The sinking D export flux depends linearly on D, however the flux to higher trophic levels and aggregation terms are nonlinear and so must be linearized about steady state 3 in order to perform the optimizations described in Chapter 3. The export function for the ecosystem state is approximated using a Taylor series expansion:

$$Export(\mathbf{x}_0 + \Delta\mathbf{x}) \approx Export(\mathbf{x}_0) + \nabla Export(\mathbf{x}_0)^T \cdot \Delta\mathbf{x} \tag{2.10}$$

where $\mathbf{x}_0$ is the ecosystem steady state, $\Delta\mathbf{x}$ the perturbation to this state, and ∇ the gradient operator relative to the state variables. The linearized export is thus given by the equation

$$Export = Export(\mathbf{x}_0) + 0.22\Delta P_2 + 0.21\Delta Z_1 + 0.38\Delta D \tag{2.11}$$

where ΔP_2, ΔZ_1, and ΔD are the perturbations in large phytoplankton, small zooplankton, and detritus, respectively. The export rates are computed in units of $mmolNm^{-3}d^{-1}$ and a constant C:N ratio is assumed for P_2, Z_1, and D, so comparing nitrogen export rates is equivalent to comparing the carbon export rate. The Redfield C:N ratio for phytoplankton of 106:16 is used (Redfield et al., 1963). Note that C:N may vary in time and for different forms of organic matter in the ocean, but on average it is well approximated by the Redfield ratio. Variations in the ratio are not modelled because the added complexity is not warranted or well-constrained (Sterner and Elser, 2002).

4 Model applications

This type of model has been used to simulate the ecosystem response to iron fertilization during SERIES (Denman et al., 2006), and a similar ecosystem model has been implemented in the Canadian Model of Ocean Carbon (CMOC), a global ocean carbon model (Zahariev et al., 2008). Because the CMOC is meant to simulate the carbon cycle, and global ecosystem models are computationally demanding on climate time scales, relatively simple ecosystem dynamics are assumed in the CMOC; the model includes only one functional group of zooplankton and of phy-

toplankton, and chl$a$ is explicitly modelled. In the CMOC, photosynthetic growth is potentially limited by light availability and temperature, in addition to iron and nitrogen. Although both models use the same formulation for zooplankton grazing, the grazing dynamics in the CMOC are simpler than in this study; zooplankton graze only on phytoplankton, and a quadratic Z mortality term represents grazing on Z. The CMOC model includes a quadratic aggregation term for P; aggregated P becomes D. Due to computational limitations, planktonic ecosystem models were not included in global climate models until recently. Currently, ecosystem models are being embedded in many general circulation models. Although the results of the current study only directly apply to the model being considered, these results may provide qualitative insight into the generic dynamics of other planktonic ecosystem models.

Chapter 3

Linearized dynamics and optimal perturbations

1 Introduction

Perturbations to a planktonic ecosystem model in stable steady state eventually return to equilibrium if they are small enough, but may grow transiently. Perturbations that optimize the ecosystem state at fixed times under some measure, such as export flux, may be determined using linear theory. These perturbations may grow transiently under the desired measure, that is, the perturbation configures the ecosystem in a way that produces a large future response. Because planktonic ecosystems are potential sinks for atmospheric carbon, the perturbation that optimizes the total export of POC from the ecosystem as it returns to steady state, termed "integrated export", is also of interest. In this Chapter, the theory necessary for these optimizations is presented, and is used to determine these optimal perturbations.

2 Theory

The system of Equations 2.1 - 2.5 can be expressed as the autonomous system of first order ordinary differential equations

$$\frac{d\mathbf{x}}{dt} = \mathbf{f}(\mathbf{x}) \tag{3.1}$$

where $\mathbf{x}$=(P_1, P_2, Z_1, D, N) is the state vector. The dynamics of a small perturbation around a fixed point $\mathbf{x}_0$, $\Delta\mathbf{x} = \mathbf{x} - \mathbf{x}_0$, can be described by the linearized dynamics

$$\frac{d}{dt}\Delta\mathbf{x} = \mathbf{A}\Delta\mathbf{x}, \tag{3.2}$$

where $\mathbf{A}$ is the Jacobian of $\mathbf{f}(\mathbf{x})$ evaluated at $\mathbf{x}_0$, that is

$$A_{i,j} = \frac{\partial f_i(\mathbf{x})}{\partial x_j}|_{\mathbf{x}=\mathbf{x}_0} \tag{3.3}$$

The solution of Equation 3.2 is

$$\Delta\mathbf{x}(t) = e^{At}\Delta\mathbf{x}_0 \tag{3.4}$$

Provided $\mathbf{x}$ remains sufficiently close to $\mathbf{x}_0$, the linearized dynamics will be a good approximation to the evolution of the full nonlinear system (Perko, 2001).

a. Optimizing rates

If the equilibrium $\mathbf{x_0}$ is stable, then the real parts of the eigenvalues of $\mathbf{A}$ will all be negative and small perturbations to a stable steady state will eventually converge

back to equilibrium. However, these perturbations may display transient growth over finite times if the matrix $\mathbf{A}$ is not normal (i.e. $\mathbf{A}\mathbf{A}^T \neq \mathbf{A}^T\mathbf{A}$, where $\mathbf{A}^T$ is the transpose of $\mathbf{A}$ (Farrell and Ioannou, 1996)). It is possible to solve for the perturbation that optimizes some measure of the size of the perturbation at a fixed time τ, subject to the constraint that the perturbation be of unit norm (under some metric) at time $t = 0$ (Tziperman and Ioannou, 2002). Let $\mathbf{R}$ be a matrix defining the perturbation norm to be optimized, so that the magnitude of the perturbation at time τ is given by

$$J(t) = \Delta\mathbf{x}_0^T(e^{A\tau})^T\mathbf{R}e^{A\tau}\Delta\mathbf{x}_0 \tag{3.5}$$

The optimal perturbation at time τ is defined as the initial perturbation $\Delta\mathbf{x}_0$ that maximizes $J(\tau)$ under the norm $\mathbf{R}$, subject to the constraint that the norm of this perturbation is unity under some nonsingular norm $\mathbf{S}$:

$$\Delta\mathbf{x}_0^T\mathbf{S}\Delta\mathbf{x}_0 = 1 \tag{3.6}$$

It follows from this constrained optimization problem that the optimal perturbations satisfy the generalized eigenvalue problem

$$(e^{A\tau})^T\mathbf{R}e^{A\tau}\Delta\mathbf{x}_0 = \lambda\mathbf{S}\Delta\mathbf{x}_0 \tag{3.7}$$

where λ is a Lagrange multiplier. That is, the eigenvector corresponding to the largest eigenvalue of the matrix

$$\mathbf{S}^{-1}(e^{A\tau})^T\mathbf{R}e^{A\tau} \tag{3.8}$$

will be the optimal perturbation at time τ under the norm $\mathbf{R}$. As the perturbation evolves, the amplification of the perturbation under $\mathbf{R}$ is defined as

$$Amp^2(t) = \frac{\Delta\mathbf{x}(t)^T\mathbf{R}\Delta\mathbf{x}(t)}{\Delta\mathbf{x}_0^T\mathbf{R}\Delta\mathbf{x}_0} \tag{3.9}$$

If $\mathbf{R}$ is singular, optimal perturbations may be nonunique, and will lead to infinite amplification if they are zero under $\mathbf{R}$. To prevent this infinite amplification, the eigenvalue problem may be regularized by adding a small diagonal matrix to $\mathbf{R}$ (Tziperman and Ioannou, 2002); for these optimizations, the diagonal entries of this small matrix are 10^{-9}.

In this study, the norm $\mathbf{R}$ is the matrix containing the coefficients of the squared linear export flux (Equation 2.11). The instantaneous export flux is optimized subject to the constraint that the initial biomass of the perturbation is unity, and in Section b., only in the phytoplankton state variables.

b. Optimizing integrated quantities

The above theory is used to optimize the magnitude of the instantaneous state of a system of equations under some measure. Because of the potential of planktonic ecosystems as carbon sinks, it is of interest to determine the perturbation that results in the maximum carbon export over some period of time, that is, the integrated export. Maximizing the instantaneous export flux is equivalent to maximizing its square (Equation 3.5). However, the perturbation that optimizes the integral of

the squared export flux does not necessarily result in the highest integrated export (which might involve some cancellation between positive and negative anomalies in export flux), so a different approach is required. The previous optimization problem involves a bilinear in the state vector, whereas this problem optimizes a dot product, and is linear in the state vector .

It is possible to determine the unit perturbation $\Delta\mathbf{x}_0$ that maximizes the integral of the projection of the model state on some vector $\mathbf{y} = (y_1, y_2, ..., y_n)$, where n is the dimension of the model. The quantity to be optimized is

$$I = \int_0^\infty \mathbf{y} \cdot e^{At}\Delta\mathbf{x}_0 dt \approx \Delta t \sum_{\tau=0}^{\infty} \mathbf{y} \cdot e^{A\tau\Delta t}\Delta\mathbf{x}_0 \tag{3.10}$$

where Δt is the timestep. Thus, the quantity to be maximized is

$$\Delta t \sum_{\tau=0}^{\infty} \mathbf{y} \cdot e^{A\tau\Delta t}\Delta\mathbf{x}_0 + \lambda(\Delta\mathbf{x}_0^T\mathbf{S}\Delta\mathbf{x}_0 - 1) \tag{3.11}$$

where λ is a Lagrange multiplier, and $\mathbf{S}$ is the identity matrix, as in Section a.. Let $M(\tau) = e^{A\tau\Delta t}$. Evaluating the dot product and setting the derivative with respect to $\Delta\mathbf{x}_0$ to 0 gives

$$\Delta\tilde{x}_{0j} = \sum_{\tau=1}^{\infty}\sum_{i=1}^{n} y_i M_{i,j}(\tau) \tag{3.12}$$

Setting

$$\mathbf{x}_0 = \frac{1}{|\Delta\tilde{\mathbf{x}}_0|}\Delta\tilde{\mathbf{x}}_0 \tag{3.13}$$

gives an initial perturbation of norm 1.

Note that optimizing the integrated export over the interval $[\tau - \Delta, \tau + \Delta]$ is

equivalent to optimizing the instantaneous export flux at time τ as $\Delta \to 0$.

3 Determination of optimal perturbations

a. Export flux: perturbation in all state variables

The theory in Section a. is used to find unit perturbations to the ecosystem model in steady state that maximize instantaneous export flux at fixed times[1]. These unit perturbations and their ecosystem and export responses are calculated 10 times per day for fixed times between 0.1 and 30 days, so that there is sufficient resolution to observe the dependence of optimal perturbations on optimization time. The components of these optimal perturbations as a function of optimization time are shown in Figure 3.1.

Each of these perturbations optimizes the export flux from the ecosystem at different intervals following the perturbation. For example, the ecosystem response to the perturbation that optimizes export flux at $\tau = 0.1$ days is shown in Figure 3.2. This unit perturbation optimizes instantaneous export flux immediately and results in the highest instantaneous export flux in response to any of the perturbations; this perturbation is simply the set of state variables that maximizes Equation 2.11. The export flux in response to this perturbation decreases from an initial maximum $4.9 mmol N m^{-2} d^{-1}$ to $0.1 mmol N m^{-2} d^{-1}$ around day 9; after this time, transient export flux remains low relative to the initial maximum.

There may be perturbations to the ecosystem that do not initially significantly increase export flux, but produce a large export response at a later time. This am-

[1]The initial perturbation may be restricted to certain state variables by choice of the matrix $\mathbf{S}$; in this case, no restriction is desired, and $\mathbf{S}$ is set to be the identity matrix.

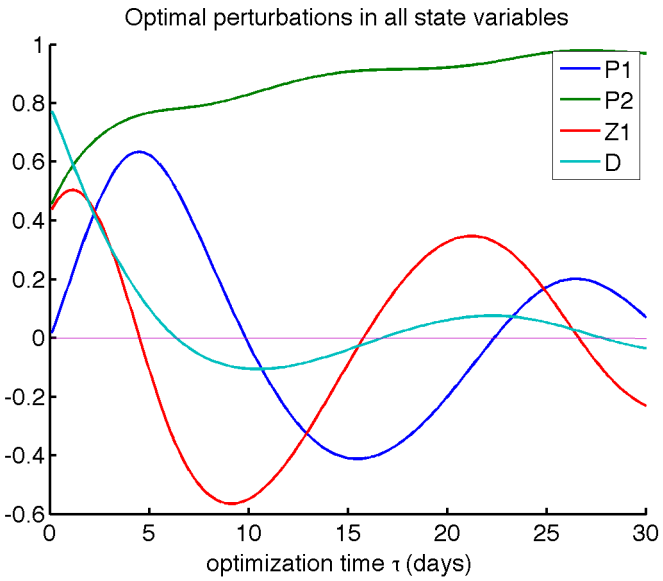

Figure 3.1: Optimal perturbations in all state variables as a function of optimization time. For each optimization time τ (the time between the perturbation and the optimized flux) there is a different set of initial conditions that produces the maximum instantaneous export flux. The optimization is performed for every 0.1 days. The perturbation Φ_{FLUX} is the set of initial conditions corresponding to $\tau = 9.3$ days.

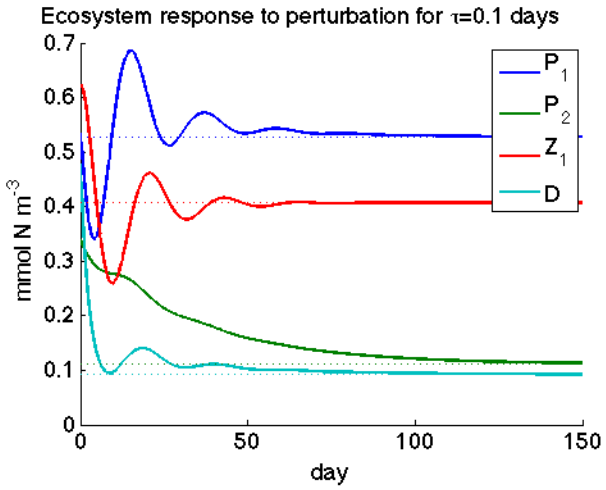

Figure 3.2: Ecosystem response to perturbation that optimizes export flux at $\tau = 0.1$ days.

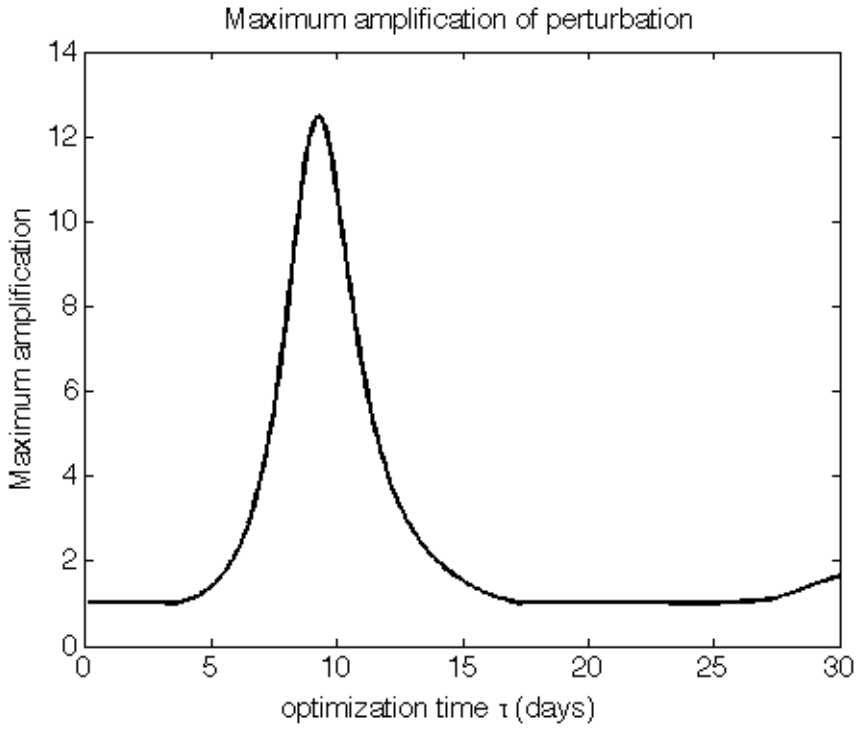

Figure 3.3: Maximum amplification of export flux following perturbations in all state variables that optimize export flux at time τ. The perturbation that gives the maximum amplification is Φ_{FLUX} and corresponds to the perturbation that optimizes export flux at $\tau = 9.3$ days.

plification of the perturbation size is measured by the magnitude of the export flux at a given time relative to the initial export flux (Equation 3.9). Unit perturbations may result in a small change in instantaneous export flux, or produce export flux an order of magnitude larger at a later time. I am interested in these perturbations because they involve the synchronization of the initial state variables in a way that produces a large future response, and thus provide insight into how different ecosystem components interact to produce certain export dynamics.

Although many of the perturbations result in no or negligible amplification (Fig-

	P_1	P_2	Z_1	D	N
Φ_{FLUX}	0.0785	0.8160	-0.5641	-0.0989	-0.0005
Φ_{FLUX-P}	0.6423	0.7665	0	0	0
Φ_{INT}	-0.0009	0.9977	-0.0296	0.0616	-0.0040
Φ_{P_2}	0	1.0000	0	0	0
$\Phi_{P_1P_2}$	0.9807	0.1955	0	0	0
Φ_{P_1}	1.0000	0	0	0	0

Table 3.1: Unit perturbations ($mmolNm^{-3}$) to steady state 3 (Table 2.3). The perturbation Φ_{FLUX} is in all state variables, optimizes instantaneous export flux, and gives high transient amplification. The perturbation Φ_{FLUX-P} is only in phytoplankton state variables, optimizes instantaneous export flux, and results in significant amplification. The perturbation Φ_{INT} optimizes integrated export flux. The perturbations Φ_{P_2}, $\Phi_{P_1P_2}$, and Φ_{P_1} are considered for comparison to the optimal perturbations

ure 3.3), the perturbation that optimizes export flux at 9.3 days results in an amplification of export by a factor of 12.5 (Equation 3.9). The ecosystem and export responses to this perturbation, denoted Φ_{FLUX} (Table 3.1), are discussed in Chapter 4.

b. Export flux: perturbation in only P_1 and P_2

In the previous section, the optimal perturbations can involve all components of the ecosystem. It is natural to ask how large a response can be generated from a perturbation in only the phytoplankton, such as a bloom. For this optimization, the theory discussed in Section a. is used to determine the perturbations in only P_1 and P_2 that optimize export flux from the ecosystem. This perturbation is realized by imposing the initial constraint

$$\Delta P_1^2 + \Delta P_2^2 + (\theta \Delta Z_1)^2 + (\theta \Delta D)^2 + (\theta \Delta N)^2 = 1 mmol N m^{-3} \tag{3.14}$$

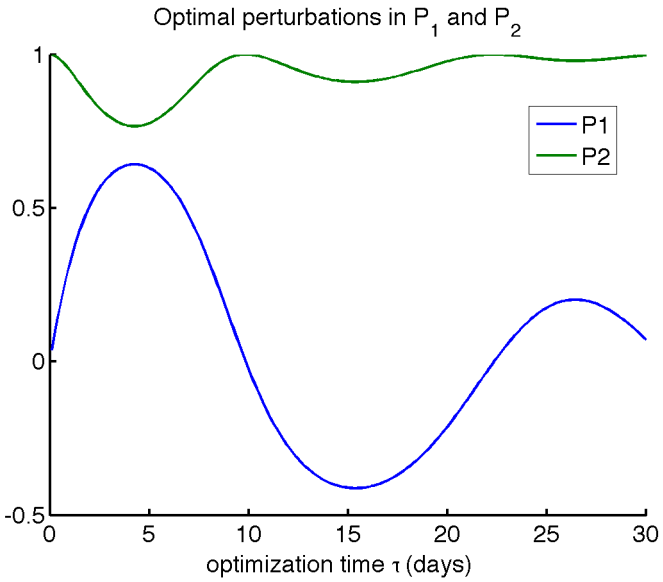

Figure 3.4: Optimal perturbations in only P_1 and P_2 as a function of optimization time. For each optimization time τ (the time between the perturbation and the optimized flux), there is a different set of initial conditions in P_1 and P_2 that produces the maximum instantaneous export rate. The perturbation Φ_{FLUX-P} is the perturbation that corresponds to $\tau = 4.3$ days.

where $\theta = 10^4$ is a factor that suppresses contributions from non-phytoplankton state variables (the coefficients of these quadratic terms are used to construct the norm $\mathbf{S}$ in Equation 3.6). The components of these optimal perturbations as a function of optimization time are shown in Figure 3.4.

Like the optimal perturbations determined in Section a., these perturbations are all primarily increases in P_2, and the P_1 components are similar between cases (Figure 3.1). The perturbation that optimizes export flux at $\tau = 4.3$ days (Figure 3.5) results in amplification of export flux by a factor of 1.5, and has the largest P_1 contribution. Although this amplification factor is small compared to the amplification of Φ_{FLUX}, export still increases by more than 50% above the initial perturbation.

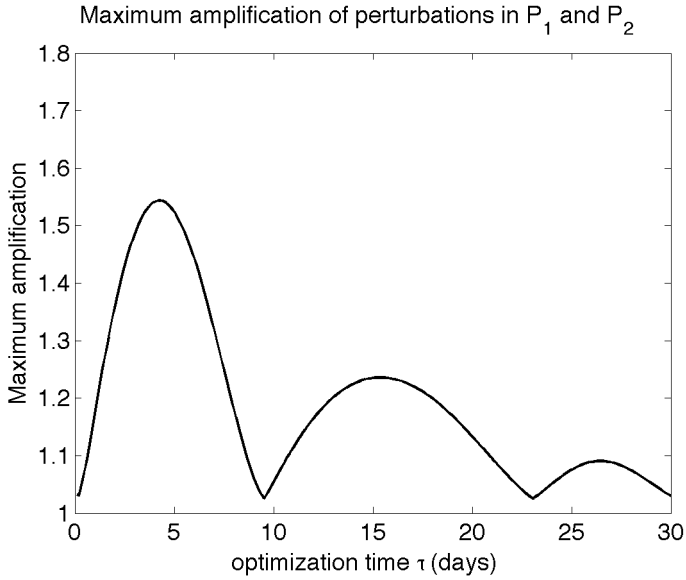

Figure 3.5: Maximum amplification following perturbations in P_1 and P_2 that optimize export flux at time τ. The perturbation that gives maximum amplification is Φ_{FLUX-P} and corresponds to the perturbation that optimizes export flux at $\tau = 4.3$ days.

The ecosystem and export responses to this perturbation, denoted Φ_{FLUX-P} (Table 3.1), are discussed in Chapter 4.

c. Integrated export

In the previous sections, instantaneous export flux is optimized at fixed times. These optimal perturbations may have little influence on the total amount of POC exported, as there is no guarantee that the transient export fluxes remain high as the ecosystem returns to equilibrium. I now characterize the unit perturbation that maximizes the integrated export, i.e., the total amount of POC exported from the ecosystem as it returns to equilibrium, Φ_{INT}, as discussed Section b..

A time step and integration time must be specified for this theory to be applied; the perturbations resulting from two different time steps and 3 different integration

		Perturbation component				
integration time	timestep	P_1	P_2	Z_1	D	N
1000 days	1 minute	-0.0008	0.9977	-0.0296	0.0616	-0.0039
1000 days	10 seconds	-0.0008	0.9977	-0.0296	0.0616	-0.0039
2000 days	1 minute	-0.0009	0.9977	-0.0297	0.0616	-0.0040
2000 days	10 seconds	-0.0009	0.9977	-0.0297	0.0616	-0.0040
3000 days	1 minute	-0.0009	0.9977	-0.0297	0.0616	-0.0040
3000 days	10 seconds	-0.0009	0.9977	-0.0296	0.0616	-0.0040

Table 3.2: Dependence of Φ_{INT} on timestep and integration time used to obtain the perturbation, obtained as described in Section b.
.

times are shown in Table 3.2.

Although, in reality, small perturbations will not affect the export flux over the entire integration time scales considered in Table 3.2, the use of a long integration time removes the sensitivity of the perturbation to the integration time used. The optimal perturbations calculated using 2000 and 3000 day integration times are the same, indicating that these integration times are sufficiently long.

In general, when analyzing integrated export response, the time steps need not be as small as considered in Table 3.2, but for the optimization problem, a small time step is required to remove the sensitivity of the perturbation to time step. Because, for each integration time, the optimal perturbations does not change between the 10 second and 1 minute time step, these time steps are sufficiently small.

The perturbation calculated using the 10 second time step and 3000 day integration time is chosen as Φ_{INT} (Table 3.1), and the ecosystem and export responses to this perturbation are discussed in Chapter 4.

d. Non-optimal perturbations

In addition to the optimal perturbations Φ_{FLUX}, Φ_{FLUX-P}, and Φ_{INT}, three non-optimal perturbations are considered (Table 3.1): an increase in only P_2 (Φ_{P_2}), a proportional increase in P_1 and P_2 ($\Phi_{P_1P_2}$), and an increase in only P_1 (Φ_{P_1}). These perturbations do not result from any optimization, i.e., they do not produce minimum or maximum export flux, but the responses to these perturbations are considered for comparison to the optimal cases.

Chapter 4

Ecosystem and Export Flux Responses to Perturbations

In this chapter, the ecosystem and export responses to the perturbations are presented. The responses to these perturbations elucidate relationships between the evolution of state variables that may not be immediately apparent from Equations 2.1-2.5. The export responses to perturbations demonstrate how different elements of ecosystems interact to produce export flux through the three export pathways: aggregation of P_2 and D, flux of P_2 and Z_1 to higher trophic levels, and sinking D.

These responses are calculated using the linearized ecosystem and export dynamics. While the linearized dynamics are insensitive to the norm of the perturbation, for presentation purposes the perturbations have been scaled to a magnitude of 0.5 $mmolNm^{-3}$ to ensure that the perturbed state variables remain non-negative. When the perturbed state variables approach zero, the linearization no longer approximates the ecosystem dynamics reasonably (as the linearization allows negative biomass).

1 Response to Φ_{FLUX}

a. Ecosystem Response.

The linearized response to Φ_{FLUX} is shown in Figure 4.1. This initial perturbation consists primarily of an increase in P_2 (Table 3.1), which monotonically decreases, taking 75 days to drop to 10% of its initial value, and a decrease in Z_1, which allows a rapid bloom of P_1, peaking at day 6 (Figure 4.1a).

The Z_1 recover due to low mortality and the abundance of available food, reaching maximum biomass at day 11. The P_1 are then grazed below steady state value to a minimum at day 17, which then leads to a local minimum of Z_1 occurring at day 22. Damped predator-prey oscillations (Volterra, 1928) continue to occur with a period of 22-23 days, with the P_1 leading the Z_1 by 5-6 days. Because the model has more than two dimensions, predator-prey oscillations are not required to be about steady state; for most of the evolution of the perturbation, the P_1 remain above steady state value as the ecosystem approaches equilibrium, while Z_1 biomass oscillates about the steady state. Because the initial perturbation in P_1 is negligible, P_1 and Z_1 are synchronized relative to their predator-prey oscillation cycle with a lag of 5 days, which allows the maximum response in P_1.

Detritus biomass, and thus export flux of sinking D, reaches a maximum at 9 days, after the initial P_1 bloom peaks but before the Z_1 attain their maximum. This maximum of D occurs before the peak Z_1 for 2 reasons: a portion of the increased P_1 being grazed down by Z_1 enters the D pool via 'sloppy feeding', and there is less grazing of Z_1 on D at this time (Equation 2.3).

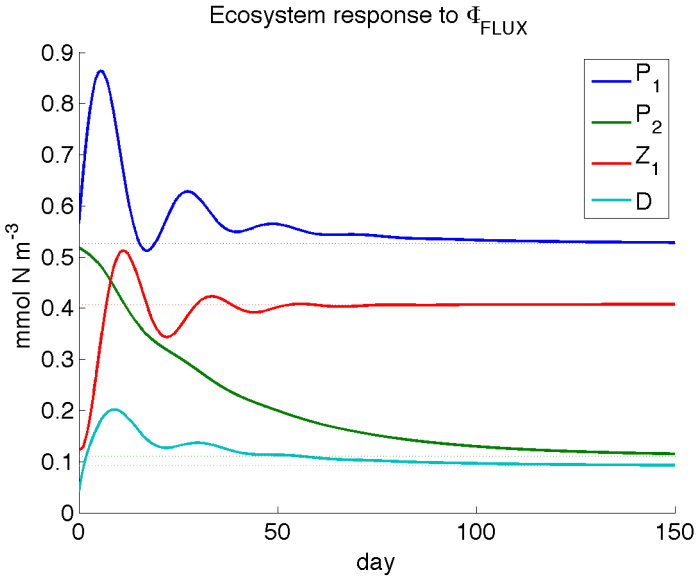

(a)

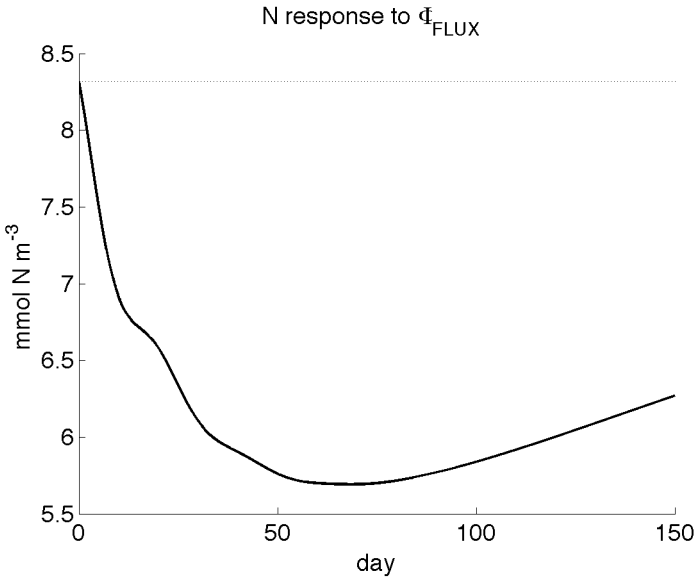

(b)

Figure 4.1: Linearized response of P_1, P_2, Z, D (a) and N (b) to Φ_{FLUX}. The perturbation Φ_{FLUX} is normalized to be of magnitude $0.5 mmol N m^{-3}$, and the perturbation is the difference between the model state and steady state (Table 2.3) at $t = 0$.

There is considerable drawdown in N (2-3 μM) with the concentration decreasing to a minimum of less than $6\mu M$ at 68.5 days (Figure 4.1b). This decay in N results from the balance between P_2 uptake, with their long decay time, and the slow, steady supply of N from below. After this time, N concentrations begin to increase, albeit slowly, taking over a year to approach the former steady state value. In fact, the model dynamics governing incoming N are unrealistic: all N recovery is through upwelling and diffusion, the model does not include horizontal mixing of nutrients. Furthermore, the model is set in a perpetual summer, with no winter deepening of the mixed layer. However, because the ecosystem is not N limited at any time, the N dynamics have no effect on the other state variables or export dynamics, which is the primary focus of this analysis.

b. Export Response.

All components of export flux increase initially in response to Φ_{FLUX} (Figure 4.2a). Export flux due to aggregation reaches a maximum at day 6, after the maximum in P_2 and before the maximum in D, and then decreases toward steady state. Export to higher trophic levels reaches a maximum at day 10, and net export increases to a maximum shortly before day 10, reflecting a compromise between export due to sinking D and flux to higher trophic levels. These maxima follow the maximum in P_1; increased grazing on P_1 produces D, which sinks and contributes to aggregation, and the increased Z_1 biomass increases the flux to higher trophic levels. The maximum aggregation occurs earliest, before the increased flux to higher trophic levels that decreases P_2. There is a second peak in export flux around day 30, and export fluxes display damped oscillations on the time scale of predator-prey interactions, in

	export flux $mmolNm^{-2}d^{-1}$		int. export ($mmolNm^{-2}$)	int. export relative to steady state (gCm^{-2})	day such that $\Delta P_2(t) = .1\Delta P_2(0)$
	min	max			
Φ_{FLUX}	2.0	4.4	350	+6.1	75
Φ_{FLUX-P}	1.9	4.4	350	+5.7	73
Φ_{INT}	1.9	4.2	370	+7.4	75
Φ_{P_2}	1.9	4.1	370	+7.4	75
$\Phi_{P_1P_2}$	1.3	3.8	300	+1.5	56
Φ_{P_1}	0.86	3.5	280	+0.02	NA
Steady State	1.8	1.8	280	0	NA

Table 4.1: Integrated, maximum, and minimum export flux, and integrated export over 150 days (1 hr timestep) in response to perturbations. The values in Column 4 are calculated using a Redfield ratio of 106:16 C:N. Export fluxes are obtained by multiplying export per unit volume by mixed layer depth (20m). Column 5 represents the P_2 decay time.

response to these oscillations in P_1 and Z_1.

Both major export events follow blooms in P_1. The maximum instantaneous export flux is $4.4mmolNm^{-2}d^{-1}$ (Table 4.1), the highest instantaneous export flux in response to any of the perturbations. Furthermore, Φ_{FLUX} is the perturbation that gives the highest export flux relative to the initial export flux of the perturbation, with an amplification factor of 12.5 (Figure 4.3). The amplification is high because the initial decrease in Z_1 decreases the flux to higher trophic levels, so that the initial perturbed export flux is marginally higher than steady state (Figure 4.2), yet the export flux reaches a maximum that is more than double steady state flux. The additional integrated export above steady state in response to this perturbation is $76mmolNm^{-2}$ ($6.1gCm^{-2}$). Aside from the initial decreased flux of sinking detritus, all export rates remain above steady state export rates, primarily because P_1 and P_2 remain above their mean values.

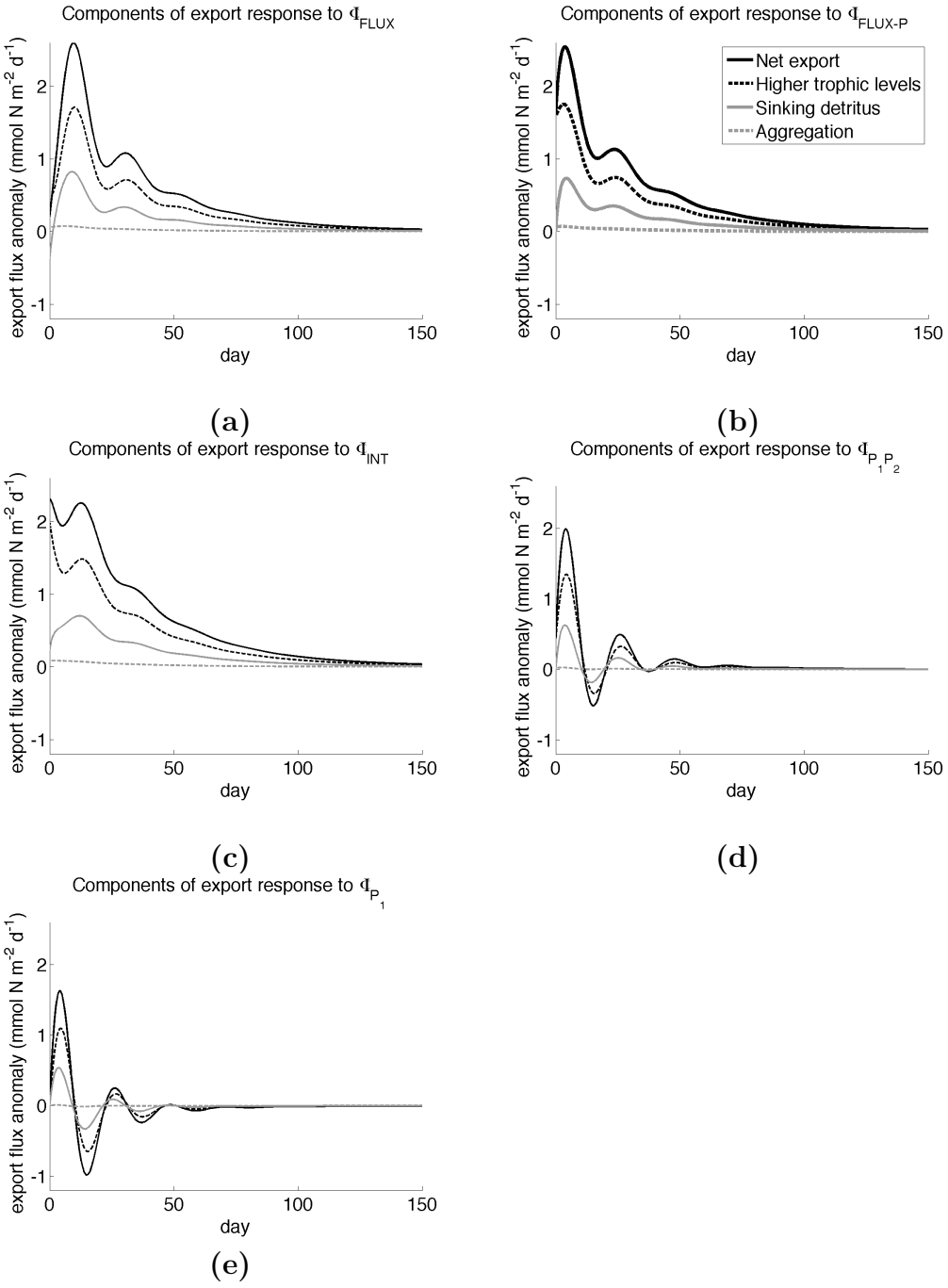

Figure 4.2: Components of export flux anomalies (net export, sinking detritus, aggregation, and flux to higher trophic levels) in response to perturbations Φ_{FLUX} (a), Φ_{FLUX-P} (b), Φ_{INT} (c), $\Phi_{P_1P_2}$ (d), and Φ_{P_1} (e)

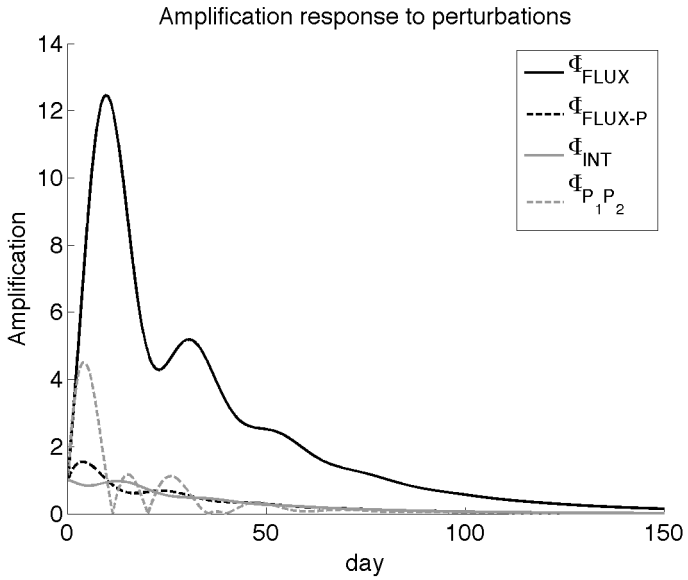

Figure 4.3: Amplification of export flux (Equation 3.9, dimensionless) in response to all perturbations except Φ_{P_1}, which has infinite amplification. The model is at steady state when amplification is zero. The time of the perturbation is $t = 0$.

2 Response to Φ_{FLUX-P}

a. Ecosystem Response.

The ecosystem response to Φ_{FLUX-P} is shown in Figure 4.4. Not surprisingly, this perturbation is an increase in both P_1 and P_2 (Table 3.1). The P_2 decay time scale is slightly shorter than in response to Φ_{FLUX}; perturbed P_2 take 73 days to decay to 10% of the initial perturbation. The response to this perturbation is very similar to the response to Φ_{FLUX} but shifted by about 6 days; like Φ_{FLUX}, damped predator-prey oscillations follow the perturbation, with P_1 remaining above steady state and Z_1 fluctuating about steady state. The microzooplankton abundance Z_1 increases in response to the increase in P_1, reaching a maximum at 5 days. Detritus increases to

a maximum at 4.3 days due to both sloppy feeding by Z_1 as the P_1 are grazed down and to mortality of P_2. The N concentration decreases to a minimum around 70.5 days, and then gradually begins to recover.

b. Export Response.

All components of export flux increase immediately following Φ_{FLUX-P} (Figure 4.2b). The net export flux reaches a maximum at 4 days. While the export flux is dominated by flux to higher trophic levels, the magnitude of this flux decreases following the perturbation; sinking detritus increases significantly following the initial perturbation, and is the main contributor to the amplification of export. The initial perturbation does not change the amount of D present in the ecosystem, but increased D due to Z_1 grazing on P_1, and P_2 mortality, result in additional export of sinking D, to a maximum at 4 days. Although the maximum amplification factor in the case of Φ_{FLUX-P} is 1.5, much smaller than in Φ_{FLUX}, the additional integrated export response to Φ_{FLUX-P} of $75 mmol N m^{-2}$ ($5.7 g C m^{-2}$) is only slightly less (Table 4.1).

3 Response to Φ_{INT}

a. Ecosystem Response

The linearized ecosystem response to the perturbation Φ_{INT} is shown in Figure 4.5. This perturbation is primarily an increase in P_2 (Table 3.1). The other components of the perturbation have a negligible effect on the ecosystem and export response; the responses to Φ_{INT} are nearly indistinguishable from the responses to a perturbation that only increases P_2, Φ_{P_2} (Table 4.1). This initial increase in P_2 decays slowly,

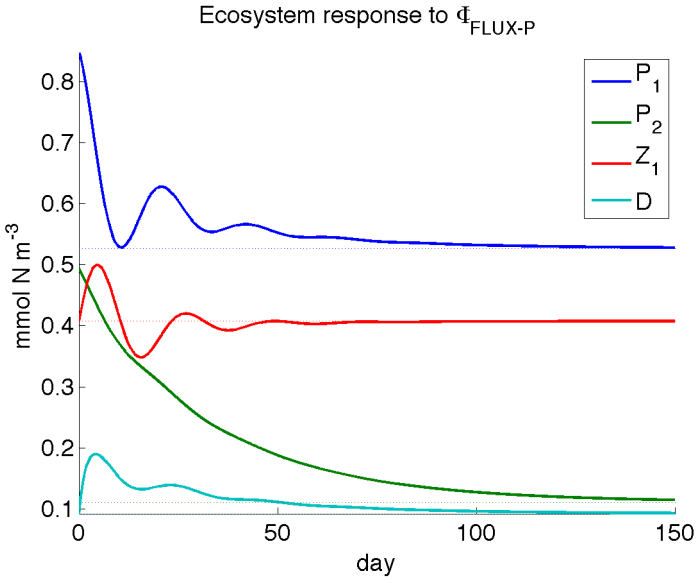

(a)

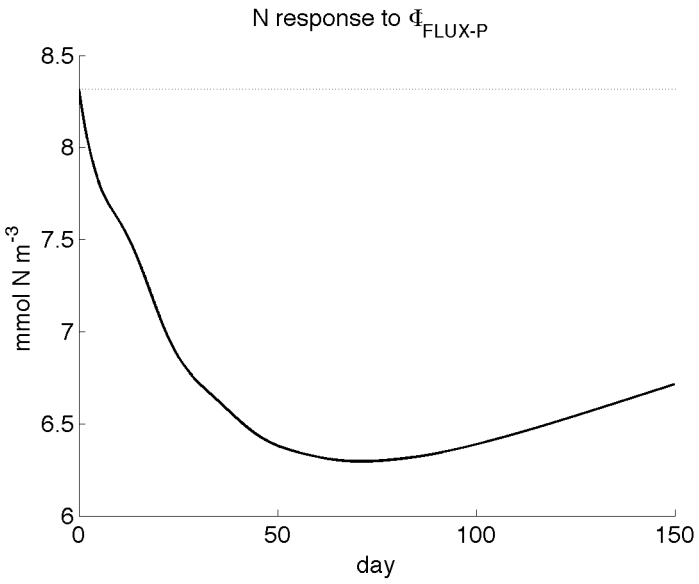

(b)

Figure 4.4: Linearized response of P_1, P_2, Z, D (a) and N (b) to Φ_{FLUX-P}

taking more than 75 days to drop below 10% of its initial value.

The initial slight decrease in Z_1 is amplified and the Z_1 biomass reduced significantly below equilibrium value to a minimum at 4.5 days. The increase in P_2 increases the overall grazing rate of Z_2, causing the decrease in Z_1. This response differs from the Z_1 increase observed following Φ_{FLUX} because Φ_{INT} has almost no P_1 component, so there is no increase in flux to Z_1 biomass to offset the increased Z_2 grazing. The decrease in Z_1 results in less predation on P_1 and D, and allows an increase in P_1 that peaks at 9.6 days. This bloom increases the food availability of the Z_1, which respond by recovering to above-steady state values, peaking at 15.8 days. Like the response to Φ_{FLUX}, damped predator-prey oscillations continue in P_1 and Z_1 with a period of 22-23 days. At no time does the P_1 biomass drop below steady state, while the Z_1 biomass oscillates about its equilibrium value.

Detritus values reach a maximum at 12.0 days. Nitrogen concentration decreases over 70 days and then slowly begins to recover. Like the N response to Φ_{FLUX}, it takes longer than a year for the N concentration to return to its steady state value.

b. Export Response.

The perturbation Φ_{INT} is primarily an increase in P_2, which results in an immediate increased flux to higher trophic levels, and thus net export (Figure 4.2c). The increased flux to higher trophic levels (Z_2 grazing) results in a decrease of Z_1, and a local minimum of both flux to higher trophic levels and net export. Damped oscillations driven by the predator-prey cycle between Z_1 and P_1 follow. Following the maxima caused by the initial P_1 bloom, all export components decrease. At no time do any of the export rates drop below steady state values.

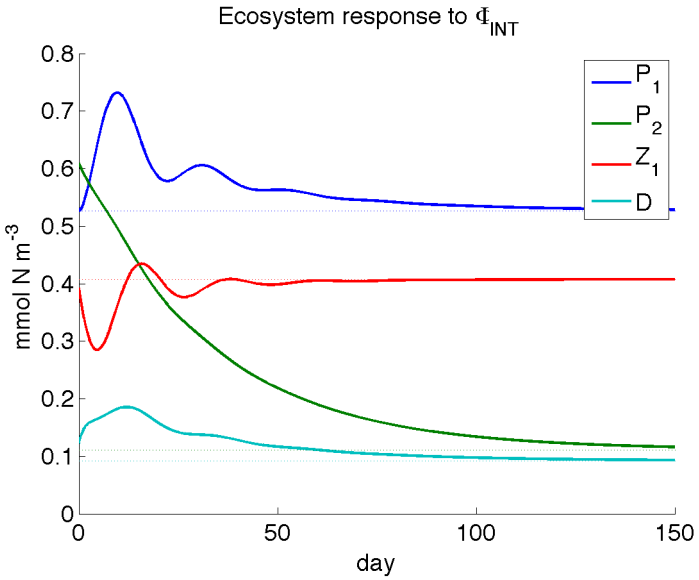

(a)

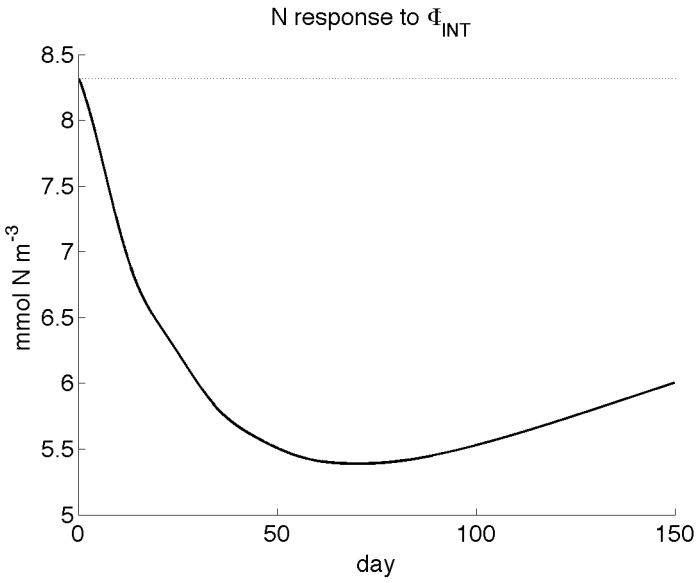

(b)

Figure 4.5: Linearized response of P_1, P_2, Z, D (a) and N (b) to Φ_{INT}

The perturbation Φ_{INT}, results in additional integrated export of $93 mmol N m^{-3}$ ($7.4 g C m^{-2}$) (Table 4.1). The maximum export flux occurs at the time of perturbation, i.e., the maximum amplification factor is less than 1. As in the response to Φ_{FLUX}, the slow decay of P_2, which is exported to higher trophic levels, is the primary reason for the large integrated export.

4 Response to proportional increase in P_1 and P_2

The optimal perturbation to only P_1 and P_2, Φ_{FLUX-P}, resulted in increased integrated export from the ecosystem relative to steady state (Table 4.1), and was primarily an increase in P_2. To investigate the dependence of perturbation evolution on non-optimal initial conditions, I consider an instantaneous bloom in both functional groups, $\Phi_{P_1P_2}$, represented by an increase in both P_1 and P_2 proportional to the phytoplankton steady state values (Table 3.1). Many conditions that improve conditions for photosynthesis for one phytoplankton functional group will similarly benefit other groups and also increase their growth rates. This perturbation increases P_1 and P_2 steady state values by some factor α, obtained by solving

$$\alpha^2 P_{1_{SS}}^2 + \alpha^2 P_{2_{SS}}^2 = 1 \tag{4.1}$$

where $P_{1_{SS}}$ and $P_{2_{SS}}$ are steady state values of P_1 and P_2, respectively. This perturbation is not the result of any optimization problem, but is considered for comparison to the optimal perturbations.

a. Ecosystem Response.

The linearized ecosystem response to $\Phi_{P_1P_2}$, shown in Figure 4.6, is dominated by the predator-prey oscillations between Z_1 and P_1. Unlike the responses to Φ_{INT} and Φ_{FLUX}, the P_1 and Z_1 both drop below steady state levels. The P_2 anomaly decays by 71% to a relative minimum at 11.7 days. Weak oscillations follow, driven by the predator-prey cycle in P_1 and Z_1 (which influences Z_2 grazing rates). P_2 values do not drop below their steady state value at any time, and it takes about 56 days for the perturbed P_2 to decrease to 10% of the initial perturbation.

The N response to $\Phi_{P_1P_2}$ is much different than the responses to Φ_{FLUX}, Φ_{FLUX-P}, and Φ_{INT}, which by construction, optimized exports. Initially N concentrations decrease as biological uptake exceeds incoming N from upwelling, reaching a minimum at 4.1 days. This change in N is much smaller than in response to previous perturbations. Afterwards, N begins to increase rapidly while overall primary production decreases, reaching a maximum in excess of its steady state concentration at 14.0 days. Following this maximum, N decreases to below equilibrium, as primary production again increases above steady state.

b. Export Response.

All of the export components increase following $\Phi_{P_1P_2}$ (Figure 4.2d), with a maximum overall amplification factor of 4.5. The integrated export in response to $\Phi_{P_1P_2}$ is $19 mmol N m^{-2}$ ($1.5 g C m^{-2}$), considerably less than the other perturbations discussed so far (Table 4.1). The maximum export flux in response to $\Phi_{P_1P_2}$ is $3.8 mmol N m^{-2} d^{-1}$, similar to the other perturbations, but unlike those previously

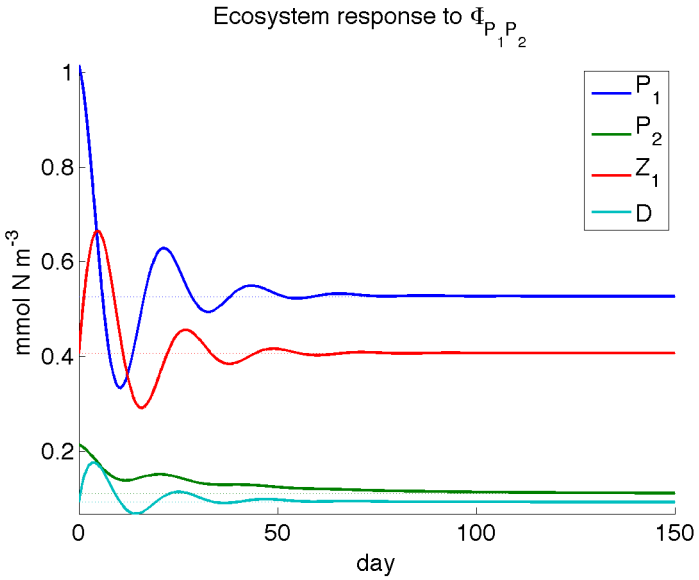

(a)

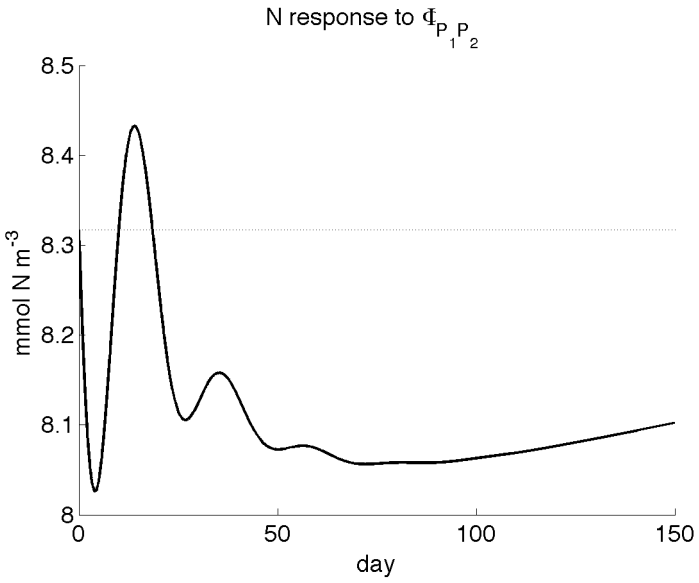

(b)

Figure 4.6: Linearized response of P_1, P_2, Z, D (a) and N (b) to $\Phi_{P_1P_2}$

discussed, the export flux oscillates around the steady state value of $1.8 mmol N m^{-2} d^{-1}$, with a minimum export flux of $1.3 mmol N m^{-2} d^{-1}$. This difference is because the P_2 contribution to increased export flux relative to steady state is not large enough to offset the decrease in D and Z_1 contributions following the declines in P_1 blooms. These minima are responsible for the relatively low integrated export, which is 20% of the integrated export due to Φ_{INT}. The overall initial increase in biomass from this perturbation reduces export flux for short time intervals.

5 Response to increase in only P_1

The perturbation $\Phi_{P_1 P_2}$ is primarily an increase in P_1 (Table 3.1). Integrated export resulting from this perturbation is low compared to that from the optimal perturbations, which are primarily in P_2, and is not much higher than the integrated export from the ecosystem at steady state. This difference leads me to investigate if increasing only P_1 results in feedbacks that actually lower the integrated export below that which occurs when the ecosystem remains at steady state over an equal time period. Like $\Phi_{P_1 P_2}$, this perturbation is a non-optimal perturbation, and will be referred to as Φ_{P_1}.

The ecosystem response to this perturbation, shown in Figure 4.7, initially resembles that to $\Phi_{P_1 P_2}$, but at 7.4 days the N anomaly becomes positive and remains slightly above zero as it decays. The concentration of N decreases when primary production is above steady state, and increases during periods when primary production is below steady state. Because, in general, export flux is highest during and following periods of high primary production, N concentration tends to decrease before periods of enhanced export flux.

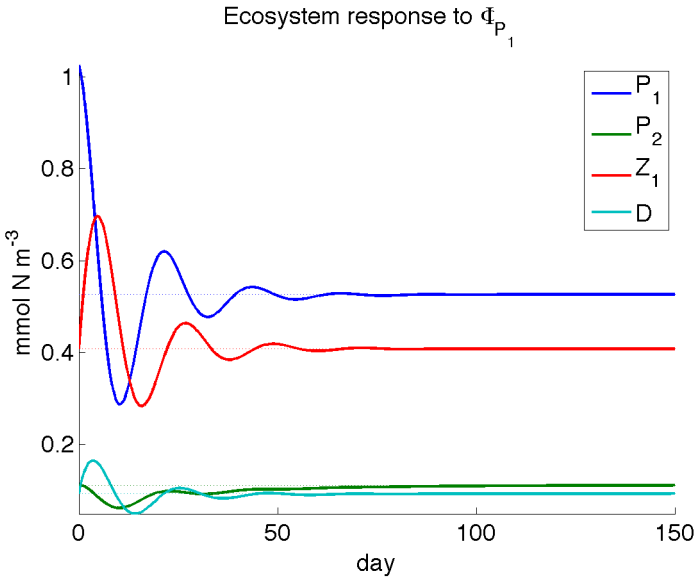

(a)

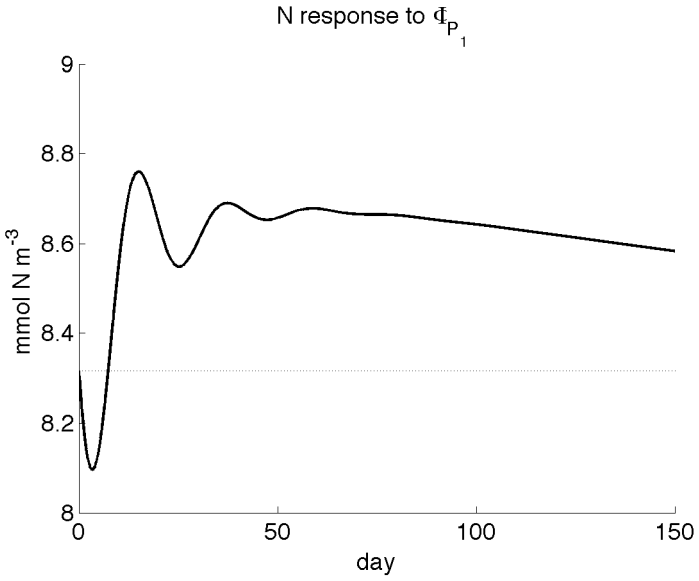

(b)

Figure 4.7: Linearized response of P_1, P_2, Z, D (a) and N (b) to Φ_{P_1}

The maximum export flux in response to Φ_{P_1} is $3.5 mmol N m^{-2} d^{-1}$ (Table 4.1), similar to the other perturbations, although the minimum export flux is the lowest at $0.9 mmol N m^{-2} d^{-1}$. There is one major export event in response to Φ_{P_1} (Figure 4.2e), which is followed by a rapid decline in export flux. The integrated export in response to Φ_{P_1} is nearly the same as integrated export from an ecosystem in steady state over an equivalent time period (Table 4.1). Thus, a perturbation that increases only P_1 does not lower integrated export.

Chapter 5

Discussion

1 Ecosystem and export dynamics

a. Common responses to optimal perturbations

The perturbations that optimize instantaneous export flux (Φ_{FLUX}, Φ_{FLUX-P}) synchronize the predator-prey cycle in Z_1 and P_1 to produce high instantaneous export flux at certain times, whereas the perturbation that optimizes integrated export (Φ_{INT}) produces the largest average export flux with little variance (Figure 4.2), i.e., there is little variability in ecosystem response to Φ_{INT}. However, there are many similarities between the ecosystem responses to these optimal perturbations. For these perturbations, the P_1 biomass remains near or above steady state, and the magnitude of oscillations in Z_1 is small relative to those in Z_1 following non-optimal perturbations $\Phi_{P_1P_2}$ and Φ_{P_1}, which keeps the Z_2 grazing pressure lower. The P_2 perturbations have a long decay time scale which may not be reasonable; it takes 70 days or longer for the P_2 perturbation to decay to 10%, and D biomass remains

above steady state (with the exception of the initial negative D component of Φ_{FLUX} (Table 3.1)). N concentrations decrease for more than 50 days, and predator-prey oscillations are not reflected in the N responses.

In contrast, for both non-optimal perturbations, $\Phi_{P_1P_2}$ and Φ_{P_1}, the magnitude of the predator prey oscillations is larger, and P_1 and D biomasses oscillate about steady state. The P_2 decay rapidly following these perturbations because high Z_1 biomass increases flux to higher trophic levels. The predator-prey cycles have a visible (but small) effect on N concentrations.

There also similarities between the export responses to the optimal perturbations; all result in integrated export significantly above steady state (Table 4.1), and the flux to higher trophic levels is the greatest contributor to export flux. It is impossible to measure grazing by mesozooplankton *in situ*, and lab experiments may not sufficiently replicate natural conditions; thus the flux of POC to higher trophic levels in nature is difficult to quantify.

The majority of export components remain above steady state in response to all optimal perturbations: anomalies in both Z_2 grazing on P_2, and sinking D remain positive (Figure 4.2), and these fluxes are large enough to offset a decrease in Z_2 predation on Z_1 when Z_1 biomass ventures below steady state. For both non-optimal perturbations, sinking D and predation by Z_2 on Z_1 oscillate about steady state, and the flux of P_2 to higher trophic levels is insufficient to offset these minima and keep net export above steady state. An increase in P_2 shifts the predator-prey oscillations: maxima and minima of Z_1 are lower, and maxima and minima of P_1 are higher than if P_2 were unchanged. Because the ecosystem model is 5-

dimensional, these oscillations do not always orbit steady state, as would occur in a 2-dimensional system. Contrary to expectations for P_2 blooms (Michaels and Silver, 1988), the contribution of aggregation to net export in response to every perturbation is insignificant as modelled (i.e., the maximum export flux due to aggregation, relative to steady state, is $< 0.1 mmol N m^{-2}$).

b. Effects of P_1 and P_2 on export dynamics.

Maximum instantaneous export fluxes occur following blooms in P_1, yet the highest integrated export is obtained from the perturbation that increases primarily P_2 (Table 3.1). The high integrated export in response to Φ_{INT} is primarily, but not entirely, due to mortality and grazing on P_2 through the duration of the bloom. The microzooplankton remain near or below steady state due to increased Z_2 grazing, allowing an extended bloom of P_1 (Figure 4.5). The maximum flux of sinking detritus is less than it is in response to Φ_{FLUX} because there is less grazing on P_1, and thus less 'sloppy feeding' contribution to D. However, the increased D decay slowly because Z_1 grazing on D remains relatively low (Figure 4.2). Together, these components contribute to enhanced export fluxes. The additional integrated export in response to Φ_{FLUX} and Φ_{FLUX-P} is $1 gC m^{-2}$ (20%) less than Φ_{INT} (Table 4.1), suggesting that as long as the perturbation is largely an increase in P_2, the other components do not significantly decrease the achievable integrated export. Although increases in primarily P_1 result in export events with high instantaneous flux ($\Phi_{P_1P_2}$, Φ_{P_1}), the Z_1 increase in response to these blooms increases Z_2 grazing, and thus decreases P_2 and integrated export.

It is believed that large phytoplankton are the primary contributor to export via

flux to higher trophic levels and sinking particles (e.g. Michaels and Silver, 1988), even in conditions where small phytoplankton are dominant. In this model, small phytoplankton do not directly contribute to export flux (Equation 2.11), but P_1 do contribute to all components of export flux indirectly. A portion of P_1 that is grazed by the microzooplankton is not assimilated and becomes D, which sinks, forms aggregates, and is grazed on by Z_1. Some of the P_1 and D biomass that is assimilated by Z_1 will be exported to higher trophic levels as Z_2 graze on Z_1. The results of Richardson and Jackson (2007) suggest that the relative contributions of all phytoplankton to export, directly and indirectly, are proportional to their net primary production, and the importance of small phytoplankton to export flux may be underestimated in current models.

c. Limitation of optimal perturbations to phytoplankton state variables.

The response to Φ_{FLUX-P} is close to the response to Φ_{FLUX}, shifted about 6 days. The perturbation Φ_{FLUX} involves a decrease in Z_1, which then allows P_1 to bloom, whereas Φ_{FLUX-P} increases P_1 initially. In both cases, the perturbations in P_1 and Z_1 are aligned to match the predator-prey cycles so that the maximum possible export occurs at their respective optimization times (Figures 4.1, 4.2, and 4.4). The minimum and maximum export fluxes resulting from these perturbations, as well as integrated export, are similar (Table 4.1), that is, the restriction of the optimal perturbation to only the phytoplankton state variables has a negligible effect on the maximum achievable export flux and integrated export as the ecosystem returns toward equilibrium. This restriction simply shifts the phase of the predator-prey

oscillations: the initial decrease of Z_1 in Φ_{FLUX} reduces the flux to higher trophic levels, and thus grazing pressure on P_2. This initial Z_1 decrease is responsible for the slightly longer P_2 decay time and the slightly higher integrated export in response to Φ_{FLUX}, i.e., Z_1 is weakly coupled with decreases in P_2 via changes in Z_2 grazing.

2 Comparison to the natural world

Steady states in ecosystem models are an idealization, and planktonic ecosystems in nature are never in steady state, but are constantly forced by atmospheric variability (both seasonal and intermittent "weather") and ocean physics (MD04). It is difficult to anticipate the timing of phytoplankton blooms due to their intermittent and transient nature, and consequently, few intensive observations of ecosystem responses to natural blooms exist in the open ocean. Iron manipulation experiments present an opportunity to control bloom timing and study ecosystem responses to these blooms in detail. In this section, I relate the results in Section 4 to observations of these experiments for two reasons: these observations are detailed and have relatively good temporal resolution, and the majority of our perturbations are increases, or blooms, in phytoplankton.

a. Magnitude of observed blooms

The perturbed changes in chl*a* are smaller than observations of phytoplankton blooms; in this study larger perturbations may cause state variables to become negative in the linearized dynamics, which is impossible in the fully nonlinear dynamics. To avoid this problem, the perturbations are set to be of magnitude $0.5 mmol N m^{-3}$; perturbed changes in chl*a* are of the same magnitude as observed blooms, yet state

variables do not become negative in response to any perturbations.

The increase in chl$a$ at t=0 is highest for Φ_{FLUX-P}, which increases chl$a$ by $1.1mg$ m^{-3} (assuming the Redfield ratio C:N=106:16, and C:chl$a$=50). For comparison, in the Sea of Japan (East Sea), spring phytoplankton blooms due to shoaling of the mixed layer and/or iron deposition have been observed to increase chl$a$ by $3-8mg$ m^{-3} (Jo et al., 2007). These changes in chl$a$ given by the perturbations and in the transient dynamics are also of the same magnitude observed following SERIES at Station P; the maximum increase in Chl$a$ concentrations observed during SERIES was $5.9mg$ chl$a$ m^{-3} (Marchetti et al., 2006).

3 Model limitations

a. Zooplankton grazing.

The mathematical formulation of zooplankton grazing functions for planktonic ecosystem models is not well constrained by observations, and several studies have investigated the sensitivity of model dynamics to these expressions (e.g. Edwards and Yool (2000), Gentleman et al. (2003), Steele and Henderson (1992)). The flux to higher trophic levels in the current model is the most significant component of ecosystem export, so sensitivities in grazing rates will be shared by export fluxes. Furthermore, the internal dynamics of the model are fully influenced by the predator-prey cycles in P_1 and Z_1. These oscillations are damped, and only occur in the transient dynamics as the ecosystem relaxes towards its stable steady state. The Lotka-Volterra-like dynamics in the Z_1 grazing function are responsible for the increase in Z_1 following blooms in P_1, so the Z_1 and Z_2 grazing formulations combined give the result that

P_2 decreases more rapidly following P_1 blooms, as observed following Φ_{P_1} and $\Phi_{P_1P_2}$. This relationship between P_1 and P_2 is a result of the Z_2 grazing dependence on both P_2 and Z_1, and is an inescapable consequence of our model framework; the realism of this relationship depends on the realism of our grazing formulations. Gentleman et al. (2003) provide an extensive discussion of grazing formulations for predators with multiple resources. This model is a homogeneous slab, and zooplankton in nature are not homogeneous in space, are able to swim, and are subject to ocean physics, such as stirring; all of these factors would be expected to damp these oscillations. Because it is difficult to observe predator-prey oscillations, it is unknown if these oscillations exist in the ocean.

b. Optimizations consider POC alone

The optimizations performed consider only particulate organic carbon leaving the mixed layer. I assume that the concentration of dissolved organic carbon (DOC) in both the mixed layer and incoming water is constant in both upper and lower layers and independent of the state of the ecosystem. At steady state, $0.6 mmol C m^{-3} d^{-1}$ is exported as POC (Table 4.1). The rate of change in DOC concentration via exchange with water blow the mixed layer, ΔDOC, is given by the equation

$$\Delta DOC = \frac{v_{uw}}{d_{ml}}(DOC_{in} - DOC_{out}) \tag{5.1}$$

where v_{uw} is the upwelling velocity ($0.1 m d^{-1}$) and d_{ml} the mixed layer depth ($20 m$). In order for the DOC contribution to export to be equivalent to the POC contribution, $\Delta DOC = \Delta POC$ and

$$-0.6 mmol C m^{-3} d^{-1} = \frac{v_{uw}}{d_{ml}}(DOC_{in} - DOC_{out}) \tag{5.2}$$

Thus, a difference in DOC concentrations of $120 mmol C m^{-3}$ at the base of the mixed layer would be required for equivalent DOC contribution to carbon export. As a difference of this magnitude is unrealistic, it is to be expected that DOC has at most a second order effect on export dynamics.

Calcifiers, primarily coccolithophorids, have been observed at Station P (Fabry, 1989); these phytoplankton form calcium carbonate shells as particulate inorganic carbon (PIC), which may be exported from the mixed layer, causing CO_2 concentrations in surface waters to increase rather than decrease (Archer, 1996, Shaffer, 1993). Because sediment trap data suggest that particulate organic carbon is the greatest contributor to export flux at 20m at Station P (Wong et al., 1999) and to higher trophic levels, I chose to neglect this inorganic component of the biological pump in my model and optimizations as most models have done in the past (e.g. Denman and Pena, 2002, Monahan and Denman, 2004) In addition, the ecology of calcifiers is poorly understood (Anderson, 2005), and currently, global models ignore or prescribe $CaCO_3$ formation as a fraction of primary production (e.g. Denman et al., 2006, Moore et al., 2001).

c. Dynamics of Large Phytoplankton

Because the growth of phytoplankton at Station P is not limited by N, it is necessary to impose a limit on photosynthetic growth and include sufficient predation to prevent complete consumption of N by model phytoplankton. The growth rate of the

phytoplankton is held constant at $0.075d^{-1}$. This growth rate implies extreme iron limitation, and is lower than is normally considered (e.g. Denman et al., 2006). The iron limitation factor L_{fe} is 0.05; when this parameter is increased above 0.1, the stable steady states are close to N limited. MD04 included potential light limitation in their formulation for photosynthetic growth (Equation 2.6); limitation by light was not included in this model version because it is set in the summer, and values obtained in MD04 for the light limitation coefficient imply that iron will be more limiting than light for my parameter set.

Complete N utilization by P_1 does not occur in this model because Z_1 biomass responds to increases in P_1. However, although the Z_2 grazing rate adjusts in response to increases in P_2, the total Z_2 biomass is held constant. The Z_2 grazing rate used in MD04 is high enough to prevent rapid blooms and complete N utilization by P_2, provided Z_2 biomass is set to the maximum of the average annual Z_2 cycle. For this reason, the high significance of flux to higher trophic levels in response to all perturbations occurs partially by construction.

For many of the perturbations, it takes more than 70 days for perturbations in P_2 to decay to 10% of their initial perturbed value (Table 4.1). This result is questionable, and this decay time scale is sensitive to the model parameters, particularly the P_2 mortality, m_{pd}, the aggregation coefficient, w_A, and the Z_2 biomass and maximum grazing rate r_c, all of which are poorly constrained. A change to these parameters that increases P_2 mortality would decrease the P_2 decay time scale and thus integrated export.

The persistence of P_2 is an important contributor to integrated export via flux

to higher trophic levels; the perturbations with the long P_2 decay time scales all give relatively high integrated export. Phytoplankton blooms are unlikely to persist on long time scales in nature because of physical variability; horizontal mixing and changes to the mixed layer depth will affect phytoplankton concentrations, and conditions for photosynthesis, such as light availability, are highly variable. However, the bloom following the Southern Ocean Iron RElease Experiment (SOIREE) persisted for more than 40 days, observed via SeaWiFS. The observed bloom may have been diatoms, but the ocean colour is unable to distinguish between functional groups; thus P_2 may persist on long time scales under certain conditions.

Because the P_2 growth rate and mesozooplankton biomass are constant, the formulation governing P_2 dynamics in the model rarely allows for increases in P_2. Physical variability is neglected in this model, as the present analysis describes what happens after these perturbations if the environment is held constant; increases in temperature, light and nutrient availability, and decreases in mixed-layer depth all improve conditions for photosynthesis and may cause blooms in P_2 (MD04).

Observations from SERIES suggest that small phytoplankton are tightly coupled with microzooplankton at Station P (Marchetti et al., 2006), as previously observed by Frost (1987). Microzooplankton may also graze on the large phytoplankton even though diatoms are rougly the same size as microzooplankton and have a silica shell. It is uncertain if this flux would be significant and likely that Z_1 graze preferrentially on P_1. Thus, as in MD04, I assume that there is no grazing by microzooplankton on diatoms. Note that Denman et al. (2006) do allow grazing of P_2 by Z_1 but the preference is low. If grazing by Z_1 on P_2 were included in my model, P_2 would be

part of the predator-prey cycles, an increase in one functional group of phytoplankton would likely lead to a decrease in the other, and the P_2 decay timescale would be shorter than in the current model.

d. Static iron limitation.

In this model, the iron limitation parameter is held constant, so the growth rate of P_2 is unchanged, even when P_2 have been persistently blooming for weeks at a time. In nature, if P_2 were blooming over an extended period of time, the phytoplankton would become more iron limited in the absence of a continual source, i.e., the iron limitation parameter L_{fe} would decrease. As a result, P_2 blooms in our model are likely more persistent than would be observed at some locations in nature. Although iron is consistently limited at Station P, some parts of the ocean are relatively iron replete. When iron limitation is considered in contemporary global biogeochemical models, iron limitation parameters vary spatially but not temporally (e.g. Zahariev et al., 2008). It is possible that these models also overestimate primary production at some locations, and thus export.

e. Linearization

The focus of this study has been the analysis of the linearized dynamics of a planktonic ecosystem model. The optimizations described in Chapter 3 require linearization of the model equations; alternatively, Monte Carlo methods could be used to gain insight into optimal perturbations without linearizing the model, but this would be computationally expensive for a 5-dimensional system of equations, and would not necessarily yield truly optimal perturbations. The resulting perturbations would be

sensitive to the magnitude of the perturbation that is being considered. The optimal perturbations determined through linear theory are independent of perturbation magnitude, and approximate the model dynamics well for sufficiently small perturbations.

The linearizations of the ecosystem and export dynamics are good approximations when the ecosystem is near steady state, but may result in significant errors for large perturbations from this state. The perturbations considered are of magnitude $0.5 mmol N m^{-3}$, and are large relative to steady state values (the magnitude of the biological state variables at steady state is $0.7 mmol N m^{-3}$, Table 2.3); these large perturbations are considered so anomalies are more directly comparable to observations. In this section, the linear and nonlinear ecosystem and export responses to two perturbations, Φ_{FLUX} and Φ_{INT}, are considered. These two perturbations are chosen for contrast; Φ_{FLUX} results in an amplification of export flux by a factor of 12.5, whereas the maximum export in response to Φ_{INT} occurs at the time of perturbation.

The linearized dynamics approximate the timing of local minima and maxima of the fully nonlinear response to Φ_{FLUX} relatively well (Figure 5.1a). There are two key differences between the linear and non-linear ecosystem dynamics: the magnitude of the predator-prey oscillations is underestimated in the linearized dynamics, and P_2 are overestimated. When Z_1 biomass is below steady state, grazing on P_1 is overestimated in the linearized dynamics; this overestimation is responsible for the difference between the linearized and nonlinearized P_1 and Z_1 during the first 20 days of the simulation. This difference is significant because Z_1 are decreased to less than

half their steady state value, and the linearized dynamics do not approximate model dynamics well for a perturbation of this magnitude. The linearization underestimates grazing on P_2, and the P_2 decay time scale is shorter (about 15 days) in the nonlinear dynamics; this time scale is more realistic than the 70 day decay time in the linearized evolution of P_2.

With the exception of P_2, the linearized ecosystem dynamics approximate the response to Φ_{INT} well (Figure 5.1b). Again, P_2 biomass is overestimated in the linear dynamics.

Figure 5.2 shows the export response to Φ_{FLUX} and Φ_{INT} calculated using the linear and nonlinear export functions. These responses both use the linearized ecosystem dynamics to ensure that any difference between cases is only due to the linearization of the export function. The linearized export function results in an underestimation of export flux for both perturbations. This underestimation is primarily because P_2 is above steady state, and because the P_2 export rate is held constant (Equation 2.11), the P_2 contribution to export flux is underestimated. For both perturbations, the linearization of the export function does not cause significant error (less than 15%).

The net effect of the linearizations is shown in Figure 5.3. The difference between the two export calculations for Φ_{FLUX} is primarily because the amplitude of the predator prey oscillations is underestimated in the linearized dynamics. The primary differences between the two calculations for Φ_{INT} occur because P_2 are overestimated in the linear dynamics, and the errors introduced by the two linearizations act in opposition to one another. For both perturbations, the linearization of the ecosystem

dynamics, not export calculations, is the primary contributor to errors. These errors are so big because the perturbations are large; there is better agreement between the linear and nonlinear dynamics for smaller perturbations (not shown). Observed blooms described in Section a. are outside of the range where the linear dynamics are a good approximation, but the linearized dynamics still provide useful qualitative information, even for large perturbations.

The ecosystem and export responses to $\Phi_{P_1P_2}$ and Φ_{P_1} may be counterintuitive. Both the linearization of the ecosystem dynamics and export flux reasonably approximate the ecosystem response for both perturbations (not shown), and any unexpected behavior during the responses is inherent to the model dynamics and not due to the linearizations.

f. Aggregation

Aggregation is thought to be important in nature, particularly when there are large blooms of P_2, but aggregation rates are not well constrained by observations. Because the aggregation coefficient w_A is small (Table 2.2), aggregation is not a significant component of export flux in response to any of the perturbations (Figure 4.2). The value of w_A used in this study is $0.02 mmol N^{-1} m^3 d^{-1}$; an increase in w_A to $0.1 mmol N^{-1} m^3 d^{-1}$ decreases the steady state concentrations of P_2 and D slightly, but has little effect on the overall ecosystem dynamics. This parameter change has a negligible effect on the optimal perturbations, and although the aggregation components of export will be higher than in Figure 4.2, aggregation is still the smallest contributor to export flux (not shown).

Aggregation increases quadratically with P_2 and D (Equations 2.2 and 2.4); be-

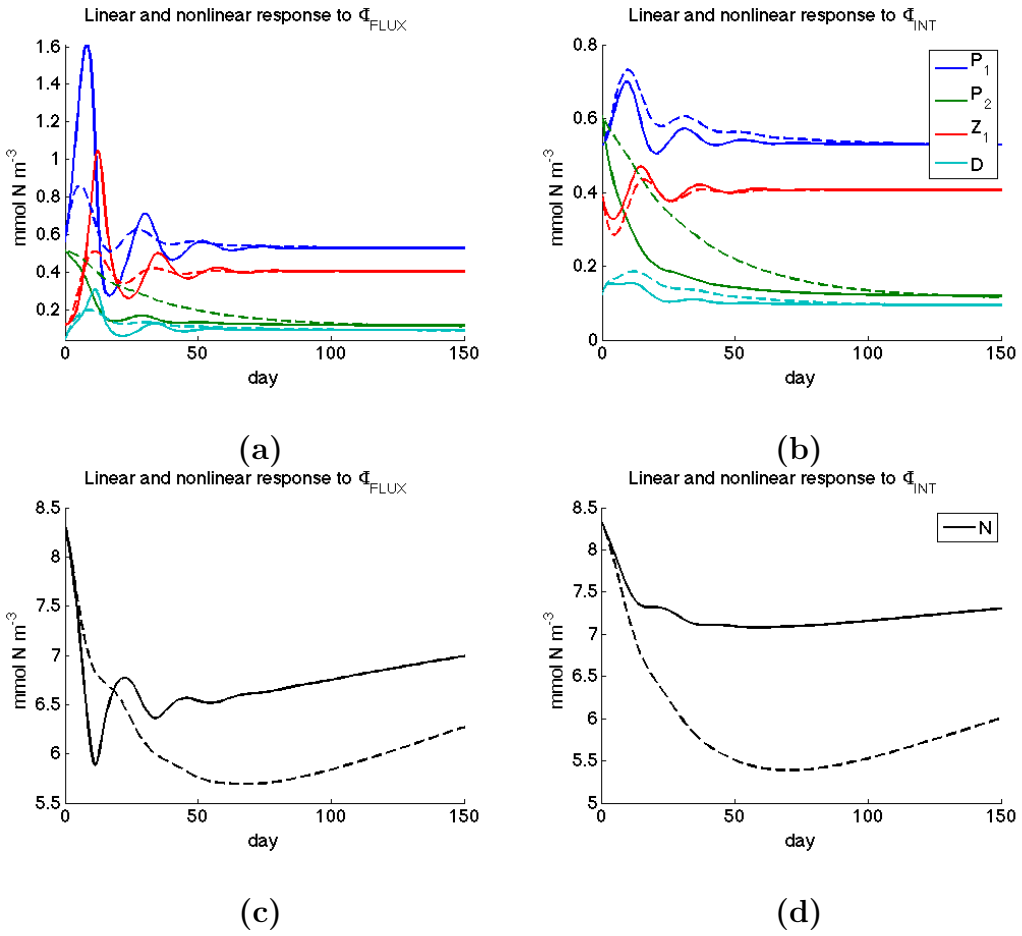

Figure 5.1: Nonlinear (solid) and linear (dashed) ecosystem response to Φ_{FLUX} (a), Φ_{INT} (b) and nitrogen response to Φ_{FLUX} (c) and Φ_{INT} (d). Perturbation magnitude is $0.5 mmol N m^{-3}$

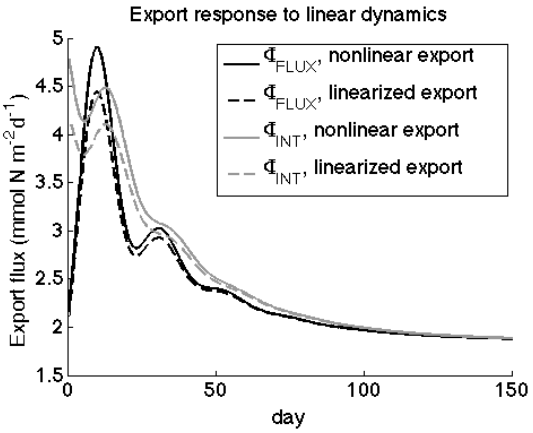

Figure 5.2: Linear and nonlinear export responses to Φ_{FLUX} and Φ_{INT}, calculated using the linearized ecosystem dynamics

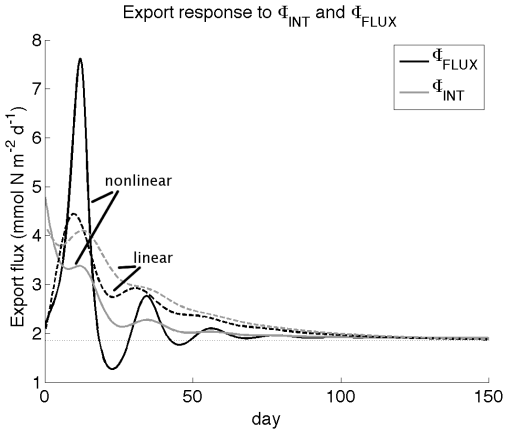

Figure 5.3: Net effects of linearizations on export responses to Φ_{FLUX} and Φ_{INT}, calculated using the nonlinear dynamics with nonlinear export function (solid) and linear dynamics with linear export function (dashed)

cause aggregation export terms are linearized about a steady state with low P_2 and D biomass (Table 2.3), P_2 and D contributions to aggregation are underestimated when these state variables are much higher than steady state (e.g. following Φ_{FLUX}).

Because aggregation has little effect on the ecosystem and export dynamics, it could be removed from this ecosystem model. This change would reduce the number of nonlinear terms and result in slightly better agreement between the linear and nonlinear dynamics.

Chapter 6

Conclusions

1 Summary

The dynamics of a planktonic ecosystem model set at Station P, located in a HNLC region of the subarctic northeast Pacific, were considered. Linearizations were performed about a stable steady state, and perturbations to this equilibrium were investigated. Two of these perturbations, Φ_{FLUX} and Φ_{FLUX-P}, were constructed to result in high transient export flux of organic material from the system. In addition, Φ_{INT} was constructed to give optimal integrated export as the ecosystem relaxed towards equilibrium. The ecosystem and export responses to these perturbations provided insight into model dynamics, and the relationships between ecosystem components and export flux.

The perturbations that synchronized P_1 and Z_1 relative to their predator-prey cycle resulted in the highest transient export flux. For all perturbations, local maxima in both sinking D and flux to higher trophic levels occurred following blooms in P_1, and export flux declined rapidly following these maxima, in many cases to

local minima. In nature, large phytoplankton are thought to be the most significant contributor to export flux, however, the significant increases in D and export flux following P_1 blooms in this study suggest P_1 play a potentially important role in export flux.

All perturbations that were primarily increases in P_2 ($\Delta P_2 > 0.8$) resulted in significant integrated export above steady state, and the only significant component of Φ_{INT} was an increase in P_2. Because of physical variability, as well as challenges observing remote parts of the ocean, extended blooms in P_2 are not frequently observed in the ocean; if conditions allowed for a persistent bloom in P_2, fertilizing P_2 may be an efficient way of fixing and sequestering CO_2. Large phytoplankton did not increase transiently in response to any perturbations, but did persist on long time scales. The persistence of P_2 was one reason that integrated export was high in response to Φ_{FLUX}, Φ_{FLUX-P}, and Φ_{INT}, as P_2 continued to bloom and be exported. However, any transient increase in export flux was due to declining blooms of P_1, and the initial increase of P_2 in Φ_{INT} actually resulted in a bloom in P_1 due to reduced grazing pressure by Z_1.

Although increased P_2 reduced grazing pressure on P_1 and resulted in an overall increase in P_1 biomass (Φ_{INT}), perturbations that primarily increased P_1 increased grazing pressure by Z_2 and accelerated the decline of P_2 ($\Phi_{P_1P_2}$, Φ_{P_1}). This relationship between P_1 and P_2 is not apparent from a casual inspection of the model equations, and it is unknown if such a relationship exists in nature. Planktonic ecosystem models are currently being embedded and modified to be coupled with GCMs to predict future climate scenarios, and these ecosystem models may also

contain such unintended relationships.

Flux to higher trophic levels is the primary contributor to export flux (Figure 4.2) in response to all perturbations. In nature, this flux is difficult to measure, and as a result, our model formulation of this flux is not well constrained by observations. Thus, my results are sensitive to the part of the model that has the fewest supporting data; other ecosystem models, including those imbedded in general circulation models (GCMs) may share this sensitivity. Transient increases in flux to higher trophic levels resulted from increased Z_1 following P_1 blooms. An increase in D biomass occurred following all perturbations, and sinking D is a significant contributor to export flux. Furthermore, my analysis also shows that for this model, it is not possible for aggregation (marine snow) to be a significant contributor to export flux for blooms of moderate size.

2 Directions of future research

This analysis yields relationships between state variables that are not obvious. It would be useful to investigate how export dynamics would change were a different ecosystem model used, particularly a model with different grazing formulations and trophic interactions, and those used with GCMs. Results could elucidate key differences between models, and if a variety of different models give similar results, this agreement could lend credence to my conclusions.

A natural extension of this study is to perform a similar analysis to an ecosystem model that includes different carbon compounds, and a functional group of calcifying phytoplankton. These components are included in models of a changing ocean (e.g. ocean acidification, Orr et al., 2005); this analysis could provide insight into

model dynamics between calcifiers, non-calcifying phytoplankton, and grazers, and in response to instantaneous chemical changes.

This model is set in the open ocean, and the parameters are tuned for a HNLC area where the effects of nutrient limitation are assumed constant. Because the ecosystem was not N limited in steady state, the response of N to perturbations did not affect the dynamics of other state variables. This type of analysis could be used to study the transient dynamics of other open ocean regions or coastal ecosystem models, which may be limited by N, and possibly other nutrients, and are subject to different sources of perturbations.

3 Conclusion

The response of this ecosystem model to perturbations provides insight into how planktonic ecosystems may respond to natural variability, and how ecosystem models may respond to a changing environment when coupled with GCMs. Because these models are being used to predict future climate scenarios, it is important to study their internal dynamics and the effects of these dynamics on carbon fluxes in ocean models.

Bibliography

Alldredge, A. and Silver, M., 1988. Characteristics, dynamics and significance of marine snow. *Progress in Oceanography*, 20(1):41 – 82.

Anderson, T. R., 2005. Plankton functional type modelling: running before we can walk? *Journal of Plankton Research*, 27(11):1073–1081.

Archer, D., Emerson, S., Powell, T., and Wong, C., 1993. Numerical hindcasting of sea surface pCO_2 at weathership Station Papa. *Progress in Oceanography*, 32(1-4):319–351.

Archer, D. E., 1996. An atlas of the distribution of calcium carbonate in sediments of the deep sea. *Global Biogeochemical Cycles*, 10(1):159–174.

Boyd, P. and Harrison, P., 1999. Phytoplankton dynamics in the ne subarctic pacific. *Deep-Sea Research Part II: Topical Studies in Oceanography*, 46(11-12):2405 – 2432.

Boyd, P. W., Law, C. S., Wong, C. S., Nojiri, Y., Tsuda, A., Levasseur, M., Takeda, S., Rivkin, R., Harrison, P. J., Strzepek, R., Gower, J., McKay, R. M., Abraham, E., Arychuk, M., Barwell-Clarke, J., Crawford, W., Crawford, D., Hale,

M., Harada, K., Johnson, K., Kiyosawa, H., Kudo, I., Marchetti, A., Miller, W., Needoba, J., Nishioka, J., Ogawa, H., Page, J., Robert, M., Saito, H., Sastri, A., Sherry, N., Soutar, T., Sutherland, N., Taira, Y., Whitney, F., Wong, S. K. E., and Yoshimura, T., 2004. The decline and fate of an iron-induced subarctic phytoplankton bloom. *Nature*, 428(6982):549–553.

de Baar, H., Boyd, P., Coale, K., Landry, M., Tsuda, A., Assmy, P., Bakker, D., Bozec, Y., Barber, R., Brzezinski, M., Buesseler, K., Boye, M., Croot, P., Gervais, F., Gorbunov, M., Harrison, P., Hiscock, W., Laan, P., Lancelot, C., Law, C., Levasseur, M., Marchetti, A., Millero, F., Nishioka, J., Nojiri, Y., van Oijen, T., Riebesell, U., Rijkenberg, M., Saito, H., Takeda, S., Timmermans, K., Veldhuis, M., Waite, A., and Wong, C.-S., 2005. Synthesis of iron fertilization experiments: From the iron age in the age of enlightenment. *Journal of Geophysical Research Part C.*, 110(9):1–24.

Denman, K. and Pena, M., 2002. The response of two coupled one-dimensional mixed layer/planktonic ecosystem models to climate change in the NE subarctic Pacific Ocean. *Deep-Sea Research Part II: Topical Studies in Oceanography*, 49(24-25):5739–5757.

Denman, K. L., Voelker, C., Pena, M. A., and Rivkin, R. B., 2006. Modelling the ecosystem response to iron fertilization in the subarctic NE Pacific: The influence of grazing, and Si and N cycling on CO2 drawdown. *Deep-Sea Research Part II: Topical Studies in Oceanography*, 53(20):2327–2352.

Edwards, A. M. and Brindley, J., 1999. Zooplankton mortality and the dynami-

cal behaviour of plankton population models. *Bulletin of Mathematical Biology*, 61(2):303–339.

Edwards, A. M. and Yool, A., 2000. The role of higher predation in plankton population models. *Journal of Plankton Research*, 22(6):1085–1112.

Fabry, V. J., 1989. Aragonite production by pteropod mollusks in the subarctic Pacific. *Deep-Sea Research, Part A.*, 36(11):1735–1751.

Farrell, B. and Ioannou, P., 1996. Generalized stability theory. Part 1: Autonomous operators. *Journal of the Atmospheric Sciences*, 53(14):2025–2040.

Fasham, M. J. R., Modelling the marine biota. In Heimann, M., editor, *The Global Carbon Cycle*, volume 73 Supp., 457–504. Springer-Verlag, 1993.

Frost, B. W., 1987. Grazing control of phytoplankton stock in the open sub-arctic Pacific-ocean - a model assessing the role of mesozooplankton, particularly the large calanoid copepods neocalanus spp. *Marine Ecology-progress Series*, 39(1):49–68.

Gentleman, W., Leising, A., Frost, B., Strom, S., and Murray, J., 2003. Functional responses for zooplankton feeding on multiple resources: a review of assumptions and biological dynamics. *Deep-Sea Research Part II: Topical Studies in Oceanography*, 50(22-26):2847–2875.

Goldblatt, R. H., Mackas, D. L., and Lewis, A. G., 1999. Mesozooplankton community characteristics in the NE subarctic Pacific. *Deep-Sea Research Part II: Topical Studies in Oceanography*, 46(11):2619–2644.

Ianson, D., Völker, C., Denman, K. L., Kunze, E., and Steiner, N., in prep. The effect of vertical and horizontal dilution on fertilized patch experiments. *Global Biogeochemical Cycles*.

Jo, C. O., Lee, J. Y., Park, K. A., Kim, Y. H., and Kim, K. R., 2007. Asian dust initiated early spring bloom in the northern East/Japan Sea. *Geophysical Research Letters*, 34(5).

Marchetti, A., Sherry, N., Kiyosawa, H., Tsuda, A., and Harrison, P., 2006. Phytoplankton processes during a mesoscale iron enrichment in the NE subarctic Pacific: Part I-Biomass and assemblage. *Deep-Sea Research Part II: Topical Studies in Oceanography*, 53(20-22):2095–2113.

Martin, J., Gordon, R., and Fitzwater, S., 1991. The case for iron. *Limnology & Oceanography*, 36(8):1793 – 1802.

Martin, J., Gordon, R., Fitzwater, S., and Broenkow, W., 1989. VERTEX: Phytoplankton/iron studies in the Gulf of Alaska. *Deep-Sea Research Part A.*, 36(5):649–680.

Michaels, A. F. and Silver, M. W., 1988. Primary production, sinking fluxes and the microbial food web. *Deep-Sea Research Part A-Oceanographic Research Papers*, 35(4):473–490.

Monahan, A. and Denman, K., 2004. Impacts of atmospheric variability on a coupled upper-ocean/ecosystem model of the subarctic Northeast Pacific. *Global Biogeochemical Cycles*, 18(2). GB2010, doi:10.1029/2003GB002100.

Moore, J. K., Doney, S. C., Kleypas, J. A., Glover, D. M., and Fung, I. Y., 2001. An intermediate complexity marine ecosystem model for the global domain. *Deep-Sea Research Part II: Topical Studies in Oceanography*, 49(1):403–462.

Moore, J. K., Doney, S. C., and Lindsay, K., 2004. Upper ocean ecosystem dynamics and iron cycling in a global three-dimensional model. *Global Biogeochemical Cycles*, 18(4):1–21.

Orr, J. C., Fabry, V. J., Aumont, O., Bopp, L., Doney, S. C., Feely, R. A., Gnanadesikan, A., Gruber, N., Ishida, A., Joos, F., Key, R. M., Lindsay, K., Maier-Reimer, E., Matear, R., Monfray, P., Mouchet, A., Najjar, R. G., Plattner, G. K., Rodgers, K. B., Sabine, C. L., Sarmiento, J. L., Schlitzer, R., Slater, R. D., Totterdell, I. J., Weirig, M. F., Yamanaka, Y., and Yool, A., 2005. Anthropogenic ocean acidification over the twenty-first century and its impact on calcifying organisms. *Nature*, 437(7059):681–686.

Perko, L., *Differential Equations and Dynamical Systems*. Springer-Verlag, 2001.

Pitchford, J. W. and Brindley, J., 1999. Iron limitation, grazing pressure and oceanic high nutrient-low chlorophyll (HNLC) regions. *Journal of Plankton Research*, 21(3):525–547.

Pond, S. and Pickard, G. L., *Introductory Dynamical Oceanography*. Butterworth-Heinemann, 1983.

Redfield, A. C., Ketchum, B. H., and Richards, F. A., The influence of organisms on

the composition of sea-water. In Hill, M., editor, *The sea: Ideas and observations on progress in the study of the seas*, 26–77. John Wiley and Sons, New York, 1963.

Richardson, T. L. and Jackson, G. A., 2007. Small phytoplankton and carbon export from the surface ocean. *Science*, 315(5813):838–840.

Saito, H., Tsuda, A., Nojiri, Y., Nishioka, J., Takeda, S., Kiyosawa, H., Kudo, I., Noiri, Y., Ono, T., Taira, Y., Suzuki, K., Yoshimura, T., and Boyd, P. W., 2006. Nutrient and phytoplankton dynamics during the stationary and declining phases of a phytoplankton bloom induced by iron-enrichment in the eastern subarctic pacific. *Deep-Sea Research Part II: Topical Studies in Oceanography*, 53(20):2168–2181.

Sarmiento, J. L. and Gruber, N., *Ocean Biogeochemical Dynamics*. Princeton University Press, 2006.

Schmittner, A., Oschlies, A., Giraud, X., Eby, M., and Simmons, H., 2005. A global model of the marine ecosystem for long-term simulations: Sensitivity to ocean mixing, buoyancy forcing, particle sinking, and dissolved organic matter cycling. *Global Biogeochemical Cycles*, 19(3):1–17.

Shaffer, G., Effects of the marine biota on global carbon cycling. In Heimann, M., editor, *The Global Carbon Cycle*, 431–455. Springer-Verlag, Germany, 1993.

Steele, J., *The Structure of Marine Ecosystems*. Harvard University Press, 1974.

Steele, J. and Henderson, E., 1992. The role of predation in plankton models. *Journal of Plankton Research*, 14(1):157–172.

Sterner, R. W. and Elser, J. J., *Ecological Stoichiometry: The Biology of Elements from Molecules to the Biosphere*. Princeton University Press, 2002.

Truscott, J. E. and Brindley, J., 1994. Ocean plankton populations as excitable media. *Bulletin of Mathematical Biology*, 56(5):981–998.

Tziperman, E. and Ioannou, P. J., 2002. Transient growth and optimal excitation of thermohaline variability. *Journal of Physical Oceanography*, 32(12):3427 – 3435.

Volk, T. and Hoffert, M., Ocean carbon pumps - Analysis of relative strengths and efficiencies in ocean-driven atmospheric CO2 changes. In Sundquist, E. and Broecker, W., editors, *The Carbon Cycle and Atmospheric CO_2: Natural variations Archean to Present*, volume 32 of *Geophysical Monograph Series*, 99–110. AGU, Washington, D.C., 1985.

Volterra, V., 1928. Variations and fluctuations of the number of individuals in animal species living together. *ICES Journal of Marine Science*, 3:3–51.

Whitney, F. and Freeland, H., 1999. Variability in upper-ocean water properties in the NE Pacific Ocean. *Deep-Sea Research Part II: Topical Studies in Oceanography*, 46(11-12):2351–2370.

Wong, C. S., Timothy, D. A., Law, C. S., Nojiri, Y., Xie, L. S., Wong, S. K. E., and Page, J. S., 2006. Carbon distribution and fluxes during the SERIES iron fertilization experiment with special reference to the fugacity of carbon dioxide (fCO(2)). *Deep-Sea Research Part II: Topical Studies in Oceanography*, 53(20):2053–2074.

Wong, C. S., Whitney, F. A., Crawford, D. W., Iseki, K., Matear, R. J., Johnson, W. K., and Page, J. S., 1999. Seasonal and interannual variability in particle fluxes of carbon, nitrogen and silicon from time series of sediment traps at Ocean Station P, 1982-1993: relationship to changes in subarctic primary productivity. *Deep-Sea Research Part II: Topical Studies in Oceanography*, 46(11):2735–2760.

Zahariev, K., Christian, J., and Denman, K., 2008. A global ocean carbon model with novel parameterizations of iron limitation, calcification and N2 fixation: preindustrial, historical, and fertilization simulations. *Progress in Oceanography*, 77:56–82.